Photochemistry and Photobiology, 2023, 99: 716–731

Special Issue Research Article

Photodynamic Inactivation of Bacteria in Ionic Environments Using the Photosensitizer SAPYR and the Chelator Citrate†

Daniel B. Eckl[1,2*‡], Nicole Landgraf[1‡], Anja K. Hoffmann[1], Anja Eichner[2], Harald Huber[1] and Wolfgang Bäumler[2]

[1]Institute for Microbiology and Archaea Centre, University of Regensburg, Regensburg, Germany
[2]Department of Dermatology, University Hospital Regensburg, Regensburg, Germany

Received 12 May 2022, accepted 19 August 2022, DOI: 10.1111/php.13701

ABSTRACT

Many studies show that photodynamic inactivation (PDI) is a powerful tool for the fight against pathogenic, multiresistant bacteria and the closing of hygiene gaps. However, PDI studies have been frequently performed under standardized *in vitro* conditions comprising artificial laboratory settings. Under real-life conditions, however, PDI encounters substances like ions, proteins, amino acids and fatty acids, potentially hampering the efficacy of PDI to an unpredictable extent. Thus, we investigated PDI with the phenalene-1-one-based photosensitizer SAPYR against *Escherichia coli* and *Staphylococcus aureus* in the presence of calcium or magnesium ions, which are ubiquitous in potential fields of PDI applications like in tap water or on tissue surfaces. The addition of citrate should elucidate the potential as a chelator. The results indicate that PDI is clearly affected by such ubiquitous ions depending on its concentration and the type of bacteria. The application of citrate enhanced PDI, especially for Gram-negative bacteria at certain ionic concentrations (*e.g.* $CaCl_2$ or $MgCl_2$: 7.5 to 75 mmol L^{-1}). Citrate also improved PDI efficacy in tap water (especially for Gram-negative bacteria) and synthetic sweat solution (especially for Gram-positive bacteria). In conclusion, the use of chelating agents like citrate may facilitate the application of PDI under real-life conditions.

INTRODUCTION

Pathogenic viruses and antibiotic-resistant bacteria are serious threats to our society. Part of the dissemination of dangerous diseases is *inter alia* nosocomial infections. They can be defined as hospital-acquired infections (HAIs), occurring during or after hospital residence. Examples include surgical wounds, primary bloodstream or urinary tract infections (1).

In Europe, roughly 63.5% of infections with antibiotic-resistant bacteria are originating from hospital and health care settings, resulting in 72.4% of attributable deaths (2). With regards to its impact on the economy, these types of infections are causing significant losses of approximately EUR 7 billion per year for the EU (3). Typical examples are infections with methicillin-resistant *Staphylococcus aureus* (MRSA), which were estimated to be responsible for costs up to EUR 1.55 billion in 2011 in Germany alone (4). In the light of antibiotic resistance, multidrug-resistant bacteria account for a prevalence of 5.7 to 19.1 per 100 patients with HAIs (5).

In health care settings, various measures against HAIs are designed such as adequate hand hygiene, proper usage of gloves and face masks and standardized procedures for cleaning and disinfection of patient-near surfaces (6). However, compliance with hand hygiene (41%) (7) and surface disinfection (48%) (8) are persistently insufficient. Both incompliances contribute to the transmittance of resistant pathogens and HAIs. Another important topic is the hesitant implementation of antimicrobial stewardship by which the use of antibiotics should be optimized (9). Thus, the ongoing fight against HAIs and the increasing resistance of bacteria against antimicrobials requires new antimicrobials but also new antimicrobial technologies.

Photodynamic inactivation (PDI) offers a viable alternative to conventional disinfectants and medical drugs in many relevant application fields, and could thus slow the pace of resistance development (10–12). PDI requires three harmless components, a photosensitizer (PS), visible light and molecular oxygen. Examples of PS for PDI include molecules like methylene blue, rose bengal, chlorine e6, TMPyP (5,10,15,20-tetrakis(1-methyl-4-pyridinio)-porphyrin tetra(p-toluene sulfonate)) or perinaphthenone derivatives such as phenalene-1-one. Upon light absorption in the PS molecule, energy or charge may be transferred to adjacent molecules to generate reactive oxygen species (ROS), among which singlet oxygen should play an important role. In case the PS is in close contact with a bacterial cell, singlet oxygen can attack chemical double bonds of biomolecules like lipids and proteins leading to cell killing (13). Owing to its mechanisms of action, PDI should not contribute to bacterial resistance (10–12).

*Corresponding author email: daniel.eckl@ur.de (Daniel B. Eckl)
‡Daniel B. Eckl and Nicole Landgraf contributed equally to this work.
†This article is part of a Special Issue celebrating the 50th Anniversary of the American Society for Photobiology.

PDI should be considered a valuable component of new antimicrobial strategies, but PDI is inherently complex when compared to standard biocidal technologies. In contrast to a single, ready-to-use biocidal molecule, singlet oxygen and other ROS are produced *in situ* by the combined action of light, PSs and oxygen. In addition, PDI uses PSs at different concentrations and with different absorption coefficients, which show different quantum yields of ROS production when exposed to light at different wavelengths, intensities and times yielding different radiant exposures.

Firstly, the complexity of biocidal ROS generation *in situ* frequently hampers the comparison of laboratory experiments, exemplarily described by the well-known PS TMPyP. PDI of *Escherichia coli* resuspended in H_2O led to 3 $\log_{10}$ steps of cell reduction in the presence of 10 µmol L^{-1} TMPyP at a very small radiant exposure of 0.079 J cm^{-2} (14). On contrary, TMPyP immobilized on a chitosan membrane required a radiant exposure of up to 172.8 J cm^{-2} to achieve the same effect with *E. coli* resuspended in PBS (15). Another study applied 0.73 µmol L^{-1} TMPyP only, which was exposed to 2052 J cm^{-2} of light to reduce the cell count significantly (16). Furthermore, for a study targeting several organisms in wastewater, 5 µmol L^{-1} TMPyP and 14.4 J cm^{-2} were applied to reach an inactivation of about 4 $\log_{10}$ steps (17).

Secondly, the situation may worsen when it comes to PDI applications beyond laboratory tests. The step from laboratory settings to real-life applications frequently may unfold additional, technological problems. However, that step is necessary and worthwhile to leverage PDI in different fields of environmental and medical applications.

Such a step was recently performed for a new application of PDI to act as an antimicrobial coating of frequently touched surfaces in health care settings and beyond (18–20). After extensive and successful laboratory tests, a field study should verify whether the PDI technology keeps its efficacy under real-life conditions. The field study was performed in two hospitals for several months and the results of the study clearly proved that the novel photodynamic coating significantly reduced the bacterial burden on patient-near surfaces, which may reduce the risk of nosocomial transmission of pathogens (18). Unfortunately, despite the advantages of PDI coatings and its proven efficacy in field studies (18,20–22), the use of silver, copper and quaternary ammoniums are reported to be the major technologies so far, whereas the role of PDI is almost unmentioned (23,24).

For potential applications of PDI in environmental and medical fields, we developed three new classes of PSs in the past years, which are chemically based on natural PSs like phenalenones, flavins and curcumins. These PSs showed a clear antimicrobial efficacy against various bacteria independent of their type and resistance profile (18,25–32). The PSs offer features, which are important when it should come to application in the environment and medicine. The molecules were patentable and its synthesis is economic. The usual tests showed that the molecules have no toxic or mutagenic potential being bio-degradable and safe for the environment.

After the first successful tests of these PSs in bacterial solutions, the use of phenalenones was tested as a potential skin antimicrobial, which might be applied in the future to decontaminate large areas of human skin. The use of PDI to reduce the bacterial load in skin wounds was already studied using other PSs (33–35). *Ex vivo* skin was inoculated with *S. aureus*, MRSA, *E. coli*, or *Pseudomonas aeruginosa*. The subsequent irradiation yielded a reduction of bacterial cells of up to 5 $\log_{10}$ steps (36). However, the *ex vivo* study revealed that the PS concentration and the radiant exposure were clearly higher when compared to experiments in solution. Obviously, the skin surface may exhibit substances that hamper the photodynamic mechanisms to some extent and among others, different ions like Ca^{2+}, Mg^{2+} and HCO_3^- might play a role (37–39). Noteworthy, these ions are also ubiquitous in other environments like tap or waste water, in both, PDI was already studied to reduce their bacterial contamination (17,40–44).

Thus, for the present study, we focused on two potential applications of PDI, which still requires a better understanding of the parameters under real-life conditions, skin decolonization and water disinfection. Decolonization of skin and mucosa is an important measure to reduce cross-contamination and surgical site infections (45). The decolonization of skin usually involves biocidal substances like chlorhexidine, triclosan and iodine leading frequently to insufficient results (46). The mucosa requires the use of antibiotics like mupirocin. Unfortunately, most of those substances already evolved a reduced sensitivity or resistance against typical skin pathogens (47).

Also the availability of safe tap water including its disinfection is an increasing challenge and the United Nations World Water Development Report stated that nearly 6 billion people will suffer from clean water scarcity by 2050 (48). While water disinfection has effectively prevented waterborne diseases, an unintended consequence is the generation of disinfection byproducts (49), which may open the door to new and safe technologies like PDI.

Both potential application fields of PDI have in common that ions like Ca^{2+} and Mg^{2+} are ubiquitous in tap water and on the skin surface. Some ions already showed a detrimental effect on PDI that was applied to inactivate *P. aeruginosa* or *S. aureus* (50). It is assumed that such ions interact with the outer environment of the bacteria (50–52) possibly resulting in a protective layer.

To overcome the detrimental effects of ions, citrate was tested as a chelating agent in bacterial solutions. VIS-spectroscopy and measurements of oxygen concentration in solutions were applied to investigate any negative effect of citrate on the used PSs. Subsequently, the results of the optimization with citrate obtained for calcium and magnesium ion solutions were transferred to solutions reflecting possible future fields of application for PDI. With citrate, an optimized PDI of *E. coli* and *S. aureus* was therefore targeted in tap water and in synthetic sweat solution.

MATERIALS AND METHODS

Bacterial strains. Escherichia coli (DSM 1103) as Gram-negative and *S. aureus* (DSM 1104) as Gram-positive model organisms for this study were purchased from DSMZ (German Collection of Microorganisms and Cell Culture Lines, Braunschweig, Germany). All organisms were cultivated on Mueller–Hinton–Medium (53) (Carl Roth GmbH & Co. KG, Karlsruhe, Germany) at 37°C and 100 rpm overnight.

Preparation of ionic solutions, synthetic sweat and tap water. Calcium chloride and magnesium chloride, both purchased from Carl Roth GmbH & Co. KG, were prepared in stock concentrations of 150, 15 and 1.5 mmol L^{-1}. Synthetic sweat solution (54,55) contained 85.56 mmol L^{-1} sodium chloride (Carl Roth GmbH & Co. KG), 0.72 mmol L^{-1} calcium chloride (Carl Roth GmbH & Co. KG), 0.13 mmol L^{-1} magnesium chloride (Carl Roth GmbH & Co. KG), 0.02 mmol L^{-1} zinc chloride (Merck KgaA, Darmstadt, Germany),

9.39 mmol L^{-1} L-histidine (Sigma-Aldrich Cooperation, St. Louis, MO), 6.84 mmol L^{-1} sodium lactate (Carl Roth GmbH & Co. KG) and 19.65 mmol L^{-1} urea (Carl Roth GmbH & Co. KG). Additionally, the synthetic sweat solution was also prepared without histidine. In all cases, ultra-pure water with a conductance >18 Ω was used as a solvent, hereafter simply referred to as H_2O. The pH value of calcium chloride and magnesium chloride solutions was adjusted to seven. Then, the solutions were filled into serum bottles, plugged, sealed, degassed and gassed with N_2 thrice and autoclaved at 121°C for 20 min at 2 bar. The solutions were then stored in the dark at room temperature. Synthetic sweat was produced freshly and sterile-filtered using 0.22 µm mixed cellulose ester-based filters (Carl Roth GmbH & Co. KG) and stored at 4°C for a maximum of 2 days. Tap water was supplied by REWAG, Regensburg, Germany (56) and sterile filtered as mentioned before. The ionic composition of the tap water is provided in Table S1.

Photosensitizers. SAPYR—a phenalenone-based PS with a quantum yield of at least 99% (25)—was purchased from TriOptoTec GmbH Regensburg, Germany. The PS was dissolved in H_2O yielding concentrations of 10, 20 and 100 µmol L^{-1}. When experiments with sodium citrate (Merck KgaA) were conducted, the PS was dissolved in sodium citrate solution (pH = 7) in concentrations of 3, 30 and 300 mmol L^{-1}.

Chemical assays via vis-spectroscopy. To investigate the effect of the chelating agent in combination with different ion solutions on SAPYR, chemical assays *via* vis-spectroscopy were conducted. The 100 µL of 100 µmol L^{-1} of PS dissolved in 300 mmol L^{-1} sodium citrate were mixed with 100 µL of 150 mmol L^{-1} of $CaCl_2$ or $MgCl_2$ solution, tap water, or synthetic sweat and pipetted into wells of a 96-well-plate. The absorption spectrum of the specimens was determined in a wavelength range from 300 to 550 nm using a spectral photometer (CLARIOStar, BMG, LABTECH GmbH, Ortenberg, Germany). The measurements were implemented once without exposure to light and subsequently after 30, 60, 300 and 600 s of illumination. A light source (blue_v, Waldmann GmbH, Villingen-Schweningen, Germany) with a radiant exposure of 18 mW cm^{-2} was used (36), resulting in a total radiant exposure of 0.54, 1.08, 5.4 and 10.8 J cm^{-2}. The radiant exposure was measured with a photosensor PD300-SH (Ophir Optronics GmbH, Nienburg, Germany) and as a display device the Nova-display (Ophir Optronics GmbH). An emission spectrum of the used lamp is given in Figure S1.

Oxygen-concentration measurement. To examine, whether the chelating agents alone or in combination with different ion solutions influenced the singlet oxygen production of SAPYR, oxygen-concentration measurements were carried out. The samples were prepared as described in the section "Chemical assays via Vis-spectroscopy," but adding 1 µL of 5 mol L^{-1} imidazole, which served as a chemical singlet oxygen quencher (57). To study potential oxygen consumption along with singlet oxygen generation (58), the measurements were also carried out without the addition of imidazole. This method ensured that produced singlet oxygen was readily depleted. The oxygen concentration in the medium was detected with a fast optical sensor (Microx 4; Presens Precision Sensing GmbH, Regensburg Germany). For the first 60 s of the measurement, the sample was illuminated with a blue light source (blue_v; Waldmann GmbH, Villingen-Schweningen, Germany) with a radiant exposure of 18 mW cm^{-2} for 40 s equal to 0.72 J cm^{-2} and the quantification was continued for 540 s, which sums up the whole measurement time to 600 s. The result was recorded as the relative oxygen saturation before and after illumination [%]. For each condition, three independent measurements were conducted.

Photodynamic inactivation. The cells were harvested *via* centrifugation (13 000 ***g***, 7 min) and suspended in H_2O. The cells were washed twice and resuspended in an ion solution, tap water or synthetic sweat. The optical density of the specimens was measured using a photometer (Ultrospec 10; Amersham Biosciences, Little Chalfont, UK) at a wavelength of 600 nm and adjusted to an OD_{600} of 0.6. 25 µL of the bacterial suspension were subsequently mixed with 25 µL of PS solution in the desired concentration either with or without citrate (150, 15 or 1.5 mmol L^{-1}, depending on the concentration of the ionic solution). The mixture was incubated for 10 min in absolute darkness and was later irradiated with the light source (see section "Chemical assays via Vis-spectroscopy") at 18 mW cm^{-2} for 300 s, equal to 5.4 J cm^{-2}. The assays also included an irradiated control of the bacteria in the respective solvent without PS (light control, later on indicated as "0 µmol L^{-1}"), a non-irradiated control of the bacteria in the respective solvent without PS as an internal reference and a nonirradiated sample with the highest PS concentration applied (dark control, later on indicated as "DC"). The 20 µL of the treated samples were transferred to 180 µL of prewarmed liquid MH-medium and incubated at 37°C for 48 h at 150 rpm. The optical density was monitored in a plate reader at 600 nm in 5 min intervals with subsequent calculation of the bacterial reduction as described and validated in previous literature (31, 39, 59, 60). In brief, the doubling time was calculated as Δt_D at an optical density between 0.2 and 0.4 in the exponential growth phase, based on an untreated reference culture. The time difference in reaching the threshold value of an optical density of 0.2 by the treated samples and the untreated reference control was determined and termed Δt. The logarithmic reduction briefly called ρ was then calculated as follows:

$$\rho = \log 2^{\frac{\Delta t}{\Delta t_D}}$$

For each condition to be tested three independent measurements ($n = 3$) were conducted and mean as well as standard deviation were calculated. According to a definition by Boyce and Pittet, a reduction of 3 $\log_{10}$ steps was considered "biologically relevant" while 5 $\log_{10}$ steps correspond to an "effective disinfection" (61). Obtained inactivation values from three independent measurements were analyzed statistically *via* unpaired, two-tailed *t*-tests assuming a normal distribution and events were considered statistically significant for $P < 0.001$. The tested conditions as well as the results of the statistical analysis are given in Table S2.

RESULTS

Influence of bivalent cations on the PDI

To evaluate whether $CaCl_2$ or $MgCl_2$ may chemically modify SAPYR without or with illumination, a mixture of ions and SAPYR was examined using vis-spectroscopy and oxygen concentration measurements. The obtained results show that $CaCl_2$ or $MgCl_2$ solutions slightly influence the absorption spectrum of the PS, independent of the duration of illumination (Fig. 1A,B). After 600 s of illumination, the loss of PS concentration is around 7.0% for PS in 75 mmol L^{-1} $CaCl_2$ solution and 9.3% for 75 mmol L^{-1} $MgCl_2$. The change in oxygen concentration was likewise not strikingly altered by the addition of ions. Due to the production of singlet oxygen by SAPYR, the oxygen concentration decreased by approximately 40% after illumination (Fig. 1C,D). Dark controls of the vis-spectrum experiments (Figures S2–S11) show nearly no loss in PS concentration indicating that loss of concentration is mainly due to photobleaching upon irradiation.

However, the oxygen depletion is solely based on the reaction of singlet oxygen with imidazole in the experimental setup. Control measurements, without the addition of the singlet oxygen scavenger, showed no decline in oxygen concentration in none of the cases where $CaCl_2$ or $MgCl_2$ was tested with or without citrate, additionally dark and light controls showed no decline in oxygen concentration (Figures S12–S23). This also indicates that the chemical reactions behind the observed PS concentration depletion described beforehand do not involve oxygen.

Now, similar experiments were carried out with ions and citrate. As shown in Fig. 2 the combination of citrate with $CaCl_2$ or $MgCl_2$ solutions had some effect on the absorption spectrum of the PS (Fig. 2A,B) as again a loss in PS concentration of around 6.8% and 9.3% were observed for $CaCl_2$ solutions and $MgCl_2$, respectively. The singlet oxygen production of SAPYR in the presence of 150 mmol L^{-1} citrate (Fig. 2C,D) was not strikingly altered as compared to experiments conducted without citrate. Again, oxygen depletion is only present when imidazole is added and dark as well as light controls do also not lead to

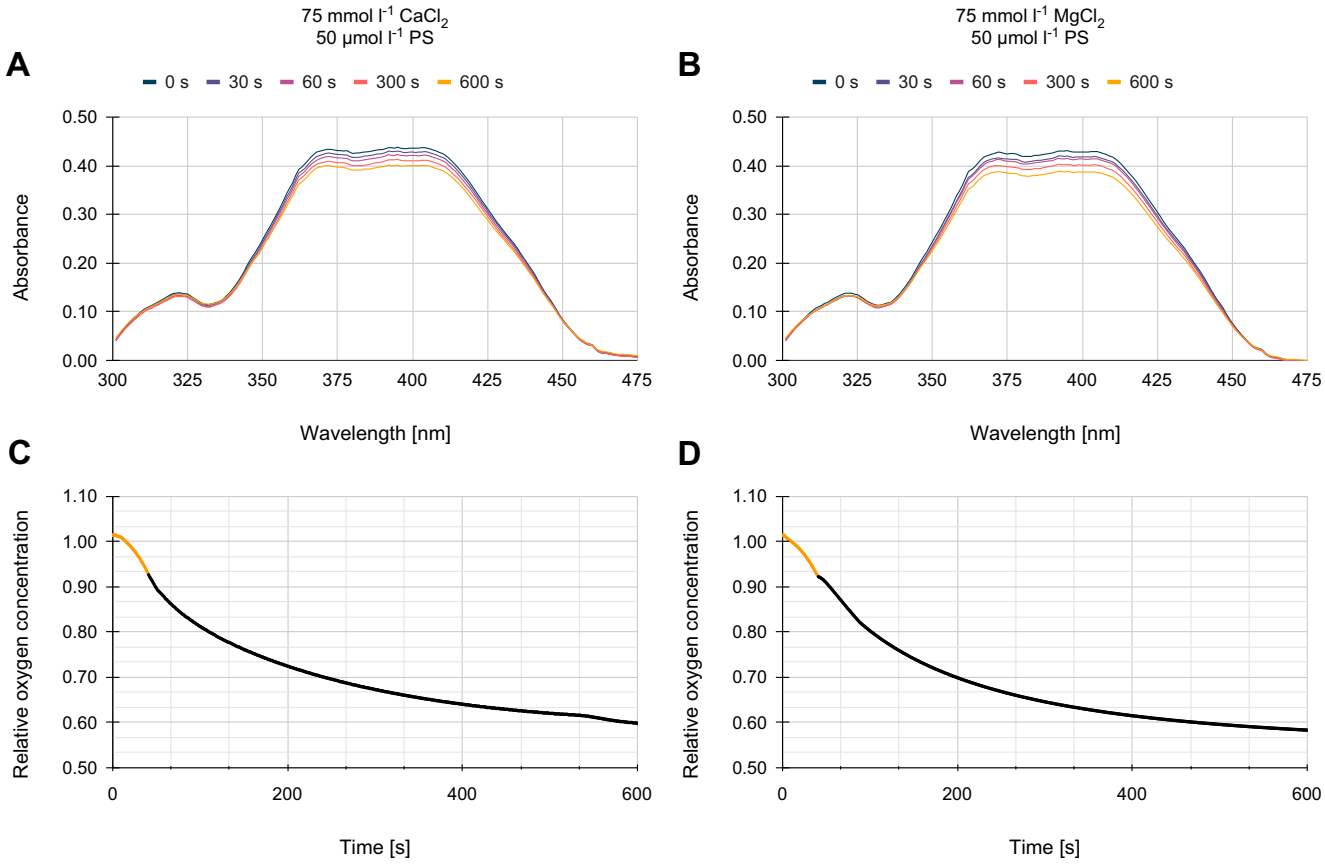

Figure 1. Effect of bivalent cations on 50 µmol L^{-1} SAPYR. The absorption spectrum of SAPYR with 75 mmol L^{-1} $CaCl_2$ (A) or $MgCl_2$ (B) after different intervals of illumination with a blue light source with a radiant exposure of 18 mW cm^{-2}. Change of the oxygen concentration after 60 s of illumination with a blue light source with a radiant exposure of 18 mW cm^{-2} of 50 µmol L^{-1} SAPYR with 75 mmol L^{-1} $CaCl_2$ (C) or $MgCl_2$ (D). The time in which the illumination was carried out is displayed as yellow datapoints.

oxygen depletion (Figures S12–S23). Citrate might be a promising chelating agent to optimize PDI as exemplarily investigated with SAPYR, *E. coli* as a Gram-negative and *S. aureus* as a Gram-positive bacterium.

Firstly, PDI was performed against *E. coli* at different concentrations of $CaCl_2$ or $MgCl_2$ as well as citrate. Concentrations of 5 and 10 µmol L^{-1} SAPYR and 0.75 mmol L^{-1} $CaCl_2$ led to a reduction of 1 and 1.5 log_{10} steps, respectively, without citrate, while the addition of citrate clearly increased the efficacy to 3.1 and 4.4 log_{10} steps, respectively (Fig. 3A). When increasing the SAPYR concentration to 50 µmol L^{-1} SAPYR, reduction of *E. coli* viability was 6 log_{10} steps, independent of the presence of citrate.

The tenfold increased $CaCl_2$ concentration of (7.5 mmol L^{-1}) revealed a clearer inhibition of PDI against *E. coli*. SAPYR concentrations of 5 and 10 µmol L^{-1} led to a reduction of less than 1 log_{10} steps without citrate, while the addition of citrate again increased the efficacy of PDI (Fig. 3B). The application of 50 µmol L^{-1} SAPYR again led to an efficient inactivation of up to 6 log_{10} steps.

The highest $CaCl_2$ concentration of 75 mmol L^{-1} clearly hampered PDI for all SAPYR concentrations yielding a maximum of about 1.7 log_{10} steps for 50 µmol L^{-1} PS, while the addition of citrate caused an increased efficacy of up to 3.2 log_{10} steps (Fig. 3C).

The use of $MgCl_2$ instead of $CaCl_2$ showed similar results for PDI against *E. coli*. However, the addition of citrate clearly increased the PDI efficacy (Fig. 3D,E). $MgCl_2$ in a concentration of 75 mmol L^{-1} again lowered the efficacy and experiments without citrate did not result in sufficient inactivation efficacies. On the contrary, experiments with added citrate achieved cell reductions of 4.5 log_{10} steps with 50 µmol L^{-1} of SAPYR. The 10 µmol L^{-1} of the PS led to a bacterial reduction of at least 2.5 log_{10} steps, while lower concentrations did not result in noteworthy logarithmic reductions (Fig. 3F). Therefore, in all cases where *E. coli* was resuspended in $MgCl_2$ solutions the application of citrate and PS led to enhanced photodynamic efficacy.

Secondly, the PDI experiments with *E. coli* were repeated with *S. aureus* cells yielding quite different results. Even the lowest applied $CaCl_2$ concentrations of 0.75 mmol L^{-1} caused a bacterial reduction of 6 log_{10} steps for 50 µmol L^{-1} SAPYR, while the addition of citrate surprisingly reduced the efficacy and led to a reduction of only 4 log_{10} steps. The small PS concentrations resulted in small reductions of viability (Fig. 4A). Again, for 7.5 mmol L^{-1} $CaCl_2$, 5 and 10 µmol L^{-1} SAPYR showed no relevant bacterial reduction, but a slightly increased efficacy was observed for 10 µmol L^{-1} when adding citrate. 50 µmol L^{-1} of SAPYR resulted in an efficient reduction of about 6 log_{10} steps without citrate and at least 6 log_{10} steps with citrate (Fig. 4B). For a $CaCl_2$ concentration of 75 mmol L^{-1} and without citrate,

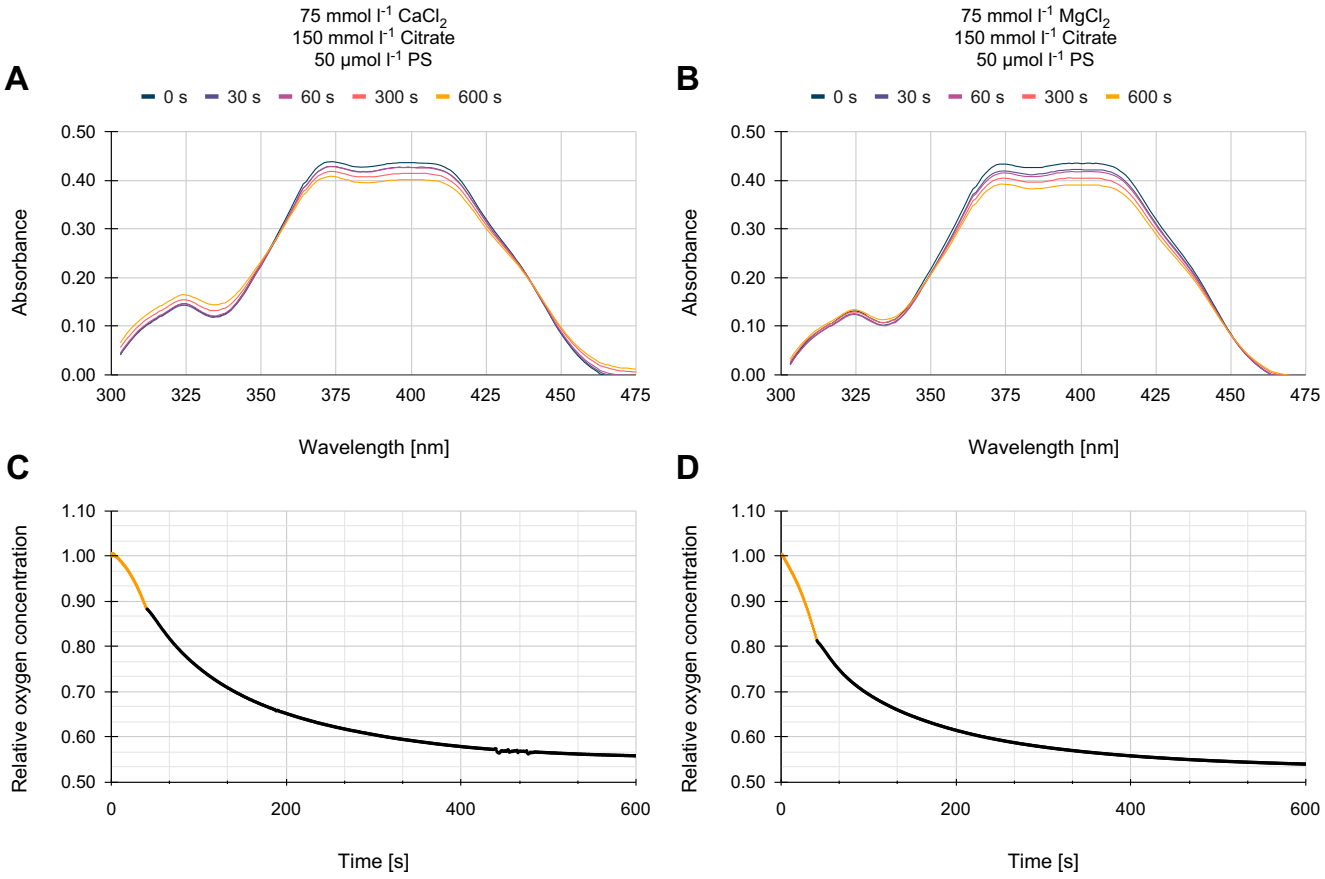

Figure 2. Effect of citrate in combination with bivalent cations on the PS SAPYR. The absorption spectrum of 50 µmol L^{-1} SAPYR with 150 mmol L^{-1} citrate and 75 mmol L^{-1} $CaCl_2$ (A) or $MgCl_2$ (B) after different intervals of illumination with a blue light source with a radiant exposure of 18 mW cm^{-2}. Change of the oxygen concentration after 60 s of illumination with a blue light source with a radiant exposure of 18 mW cm^{-2} of 50 µmol L^{-1} SAPYR with citrate in combination with 75 mmol L^{-1} $CaCl_2$ (C) or $MgCl_2$ (D) and 150 mmol L^{-1} citrate. The time in which the illumination was carried out is displayed as yellow datapoints.

the bacterial reduction was below $\log_{10}$ step for all SAPYR concentrations. The addition of citrate clearly improved bacterial reduction, especially for the highest PS concentration, and an increased efficacy with over 5 $\log_{10}$ steps of bacterial reduction was observed (Fig. 4C).

When 0.75 mmol L^{-1} of $MgCl_2$ was added to *S. aureus* suspensions, the addition of citrate did not improve the PDI effect (Fig. 4D). For 7.5 and 75 mmol L^{-1} $MgCl_2$, PDI improved in the presence of citrate (Fig. 4E,F).

Influence of tap water on PDI

A combination of different ions in solution could potentially inhibit the application of PDI outside any laboratory experiments under real-life conditions. These conditions were gradually approached by investigating the influence of tap water on PDI since it contains a variety of ions. Vis-spectroscopy showed only a small loss of concentration (9.3%) in the spectrum of SAPYR when tap water was applied (Fig. 5A). However, when citrate was added to tap water, the PS concentration decreased by about 20% (Fig. 5B). Concerning the change of oxygen concentration after illuminating SAPYR in tap water, there is also no striking alteration without (Fig. 5C) or with citrate (Fig. 5D). Measurements conducted without the addition of the artificial singlet oxygen quencher imidazole show that the oxygen depletion is based on reactions of the produced singlet oxygen with imidazole, which does not occur in measurements without imidazole and, furthermore, dark as well as light control measurements showed no decline in oxygen concentration (Figures S24–S29).

PDI against *E. coli*, being previously suspended in tap water, showed a better effect in the presence of citrate, achieving 6 $\log_{10}$ steps for 10 and 50 µmol L^{-1} SAPYR (Fig. 5E). With *S. aureus* as the test organism, the result was similar except when 10 µmol L^{-1} of SAPYR were applied. Here, the antibacterial effect was partly less efficient when citrate was added. No difference was detected for the highest PS concentration. (Fig. 5F).

Influence of synthetic sweat on PDI

To further explore the potential clinical use of PDI on the skin, the experiments were conducted in a synthetic sweat solution consisting of agents, which are typically present on human skin. The spectroscopic results indicate that the synthetic sweat severely interferes with the SAPYR since its absorption spectrum is dramatically altered after illumination independent of whether citrate was added or not (Fig. 6A,B). The spectra do not form isosbestic points as the measured values do not meet the criteria

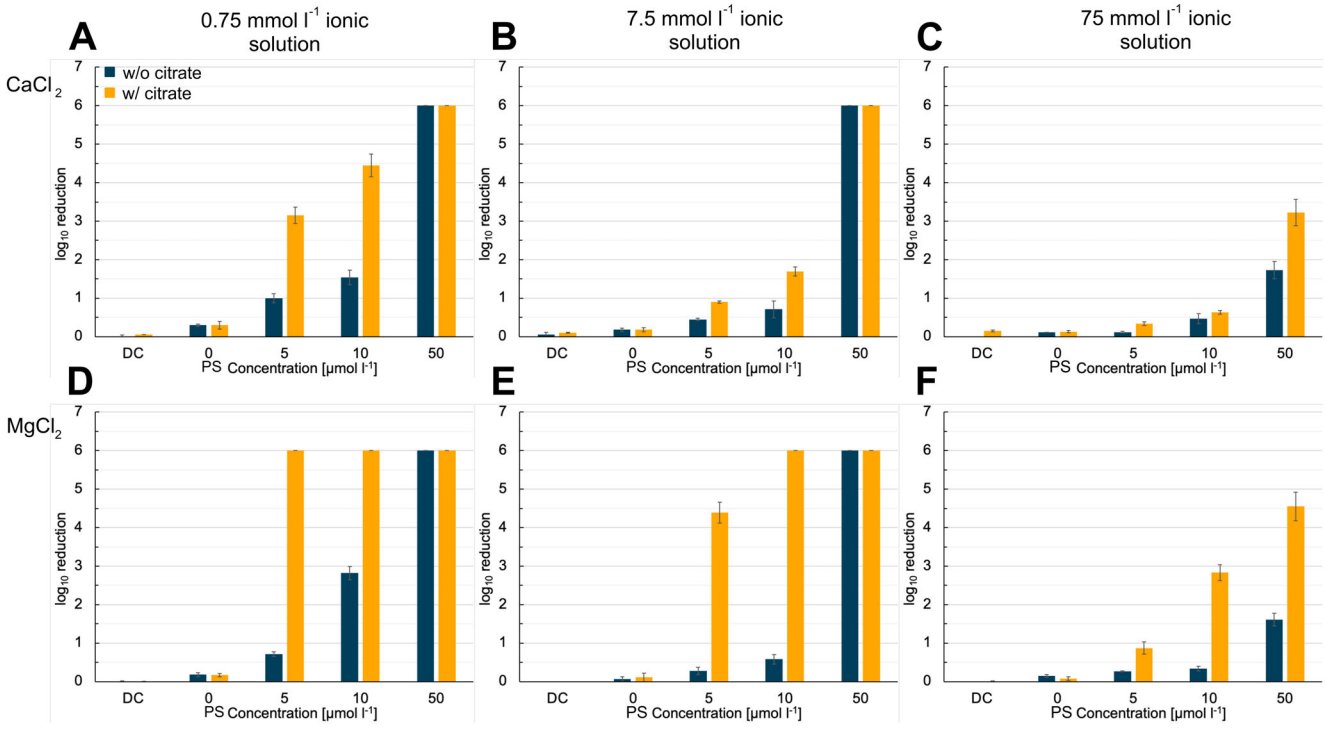

Figure 3. Calculated $\log_{10}$ reduction after the PDI of *E. coli* in presence of bivalent cations in different concentrations. PDI of *E. coli* with and without citrate in presence of 0.75, 7.5 and 75 mmol L^{-1} $CaCl_2$ (A–C) or $MgCl_2$ (D–F). Blue bars indicate results obtained without the addition of citrate, yellow bars indicate the addition of the corresponding citrate concentration of 1.5, 15 or 150 mmol L^{-1}. A and D represent a salt concentration of 0.75 mmol L^{-1}, B and E represent a salt concentration of 7.5 mmol L^{-1} and C and F represent a salt concentration of 75 mmol L^{-1}. Error bars display the calculated standard deviation out of three independent experiments. The treatment was carried out with 18 mW cm^{-2} for 300 s, equal to 5.4 J cm^{-2}.

described elsewhere (62). The change of oxygen concentration after illuminating SAPYR was not altered (Fig. 6C,D). However, the decline in oxygen concentration is partly caused by the present histidine in the reaction as measurements without imidazole showed, but still dark controls as well as light controls do not show any decline in oxygen concentration (Figures S30–S35). The PDI of *E. coli* suspended in synthetic sweat was not effective since the $\log_{10}$ reduction did not exceed 1 $\log_{10}$ step, independent of whether citrate was added or not (Fig. 6E). With *S. aureus* suspended in synthetic sweat, the bacterial reduction was slightly higher and with the addition of citrate more efficient than without (Fig. 6F). In none of the cases, a bacterial reduction exceeding 3 $\log_{10}$ steps was measured.

Influence of synthetic sweat without histidine on the PDI

To determine which component of the synthetic sweat solution was responsible for the inhibiting effect, histidine as a known chemical singlet oxygen quenching molecule was omitted from the mixture. Then, the experiments shown above were repeated accordingly. The absorption spectrum of SAPYR was not strikingly altered by the addition of synthetic sweat without histidine (Fig. 7A). When citrate was added, a slight loss of PS concentration occurred (Fig. 7B). The change of oxygen concentration after illuminating the PS was not influenced by the addition of synthetic sweat without histidine with or without citrate (Fig. 7C, D). In oxygen depletion measurements without imidazole as well as in dark and light controls no decline in relative oxygen concentration was measurable (Figures S36–S41).

PDI of *E. coli*, when suspended in synthetic sweat without histidine, was effective in achieving at least 6 $\log_{10}$ steps of bacterial reduction with or without citrate at a PS concentration of 50 µmol L^{-1}. The addition of citrate improved the bacterial inactivation only slightly with a PS concentration of 5 µmol L^{-1} (Fig. 7E). When the PDI was conducted with *S. aureus*, cell reduction was enhanced when citrate was added to the highest concentrations of SAPYR achieving around 5.5 $\log_{10}$ steps of bacterial reduction (Fig. 7F).

DISCUSSION

It is known from several investigations that different ubiquitous ions like Ca^{2+} can hamper the effectiveness of PDI (50–52). Thus, the current study aimed at the evaluation of PDI efficacy in the presence of such ions, as well as the potential improvement of PDI using chelating agents like citrate. Chelating agents generate complexes with bivalent cations and hence impeding their interaction with the outer membrane of Gram-negative bacteria or the outer cell components of Gram-positive organisms.

In the current study, the efficacy of PDI against *E. coli* increased with increasing SAPYR concentrations to a maximum of 6 $\log_{10}$ steps in the presence of low or moderate ion concentrations. However, PDI yielded less than 2 $\log_{10}$ steps in the presence of high ion concentrations. The addition of citrate clearly improved PDI in all these settings (Fig. 3).

For *S. aureus*, the efficacy of PDI also increased with increasing SAPYR concentrations and was less than 2 $\log_{10}$ steps in the presence of high ion concentrations. However, PDI yielded a

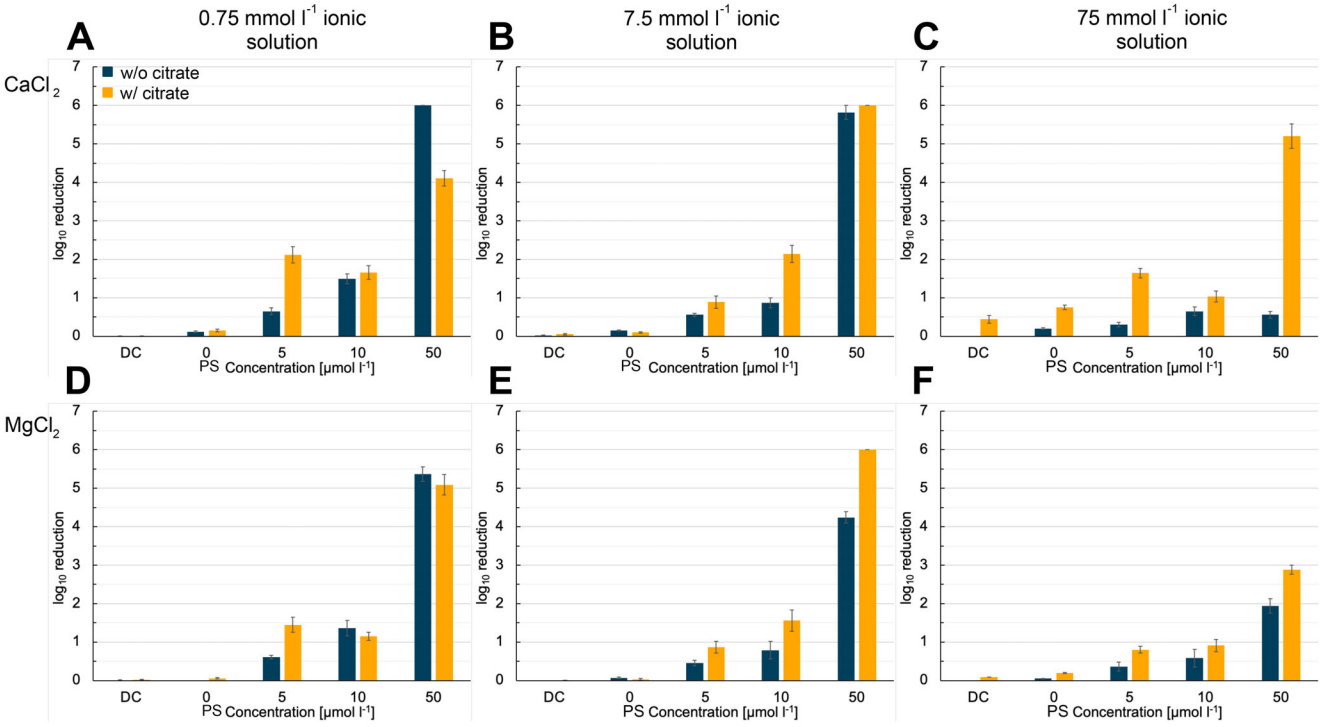

Figure 4. Calculated $\log_{10}$ reduction after the PDI of S. aureus in the presence of bivalent cations with different concentrations. PDI of S. aureus with and without citrate in the presence of 0.75, 7.5 and 75 mmol L^{-1} $CaCl_2$ (A–C) and $MgCl_2$ (D–F). Blue bars indicate results obtained without the addition of citrate, yellow bars indicate the addition of the corresponding citrate concentration of 1.5, 15 or 150 mmol L^{-1}. A and D represent a salt concentration of 0.75 mmol L^{-1}, B and E represent a salt concentration of 7.5 mmol L^{-1} and C and F represent a salt concentration of 75 mmol L^{-1}. Error bars display the calculated standard deviation out of three independent experiments. The treatment was carried out with 18 mW cm^{-2} for 300 s, equal to 5.4 J cm^{-2}.

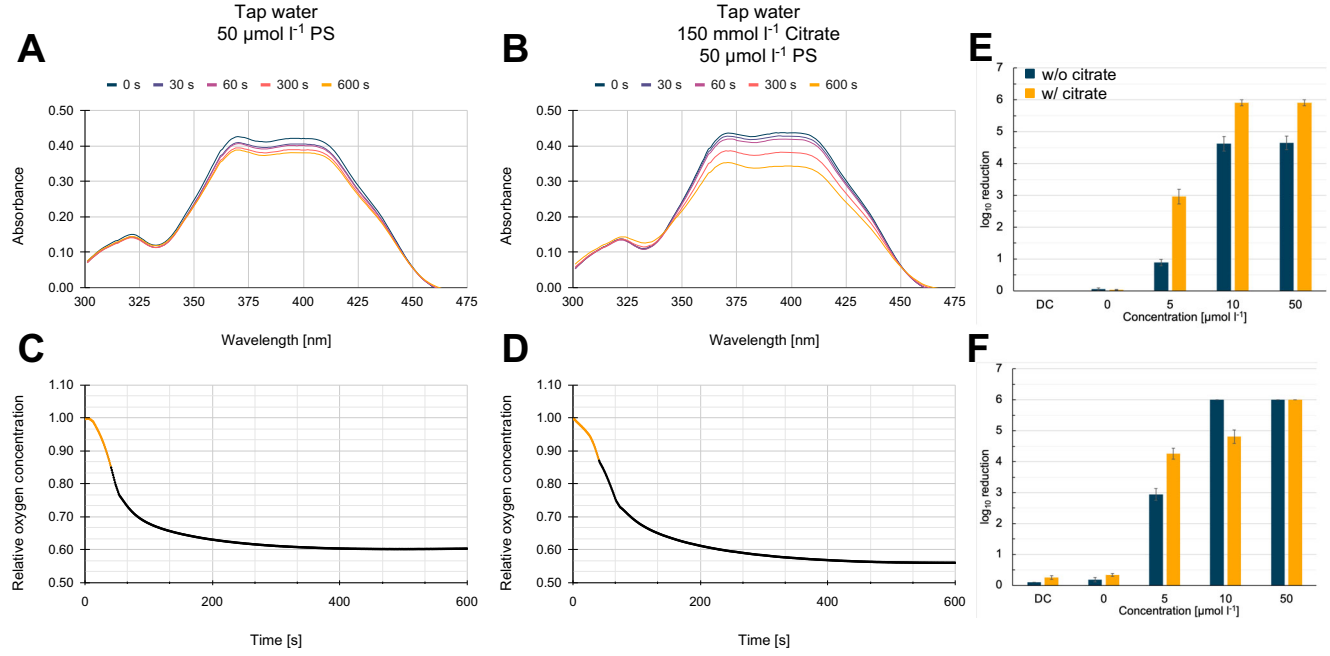

Figure 5. Investigation of the effect of tap water on the PDI. The absorption spectrum of 50 µmol L^{-1} SAPYR with tap water (A) or tap water combined with 150 mmol L^{-1} citrate (B) after different intervals of illumination with a blue light source with a radiant exposure of 18 mW cm^{-2}. Change of the oxygen concentration after 60 s of illumination with a blue light source with a radiant exposure of 18 mW cm^{-2} (indicated by yellow data points) of 50 µmol L^{-1} SAPYR with tap water (C) or tap water combined with 150 mmol L^{-1} citrate (D). Calculated $\log_{10}$ reduction after the PDI of *E. coli* (E) and *S. aureus* (F) in tap water with or without the addition of 150 mmol L^{-1} citrate. Error bars display the calculated standard deviation out of three independent experiments. The treatment was carried out with 18 mW cm^{-2} for 300 s, equal to 5.4 J cm^{-2}.

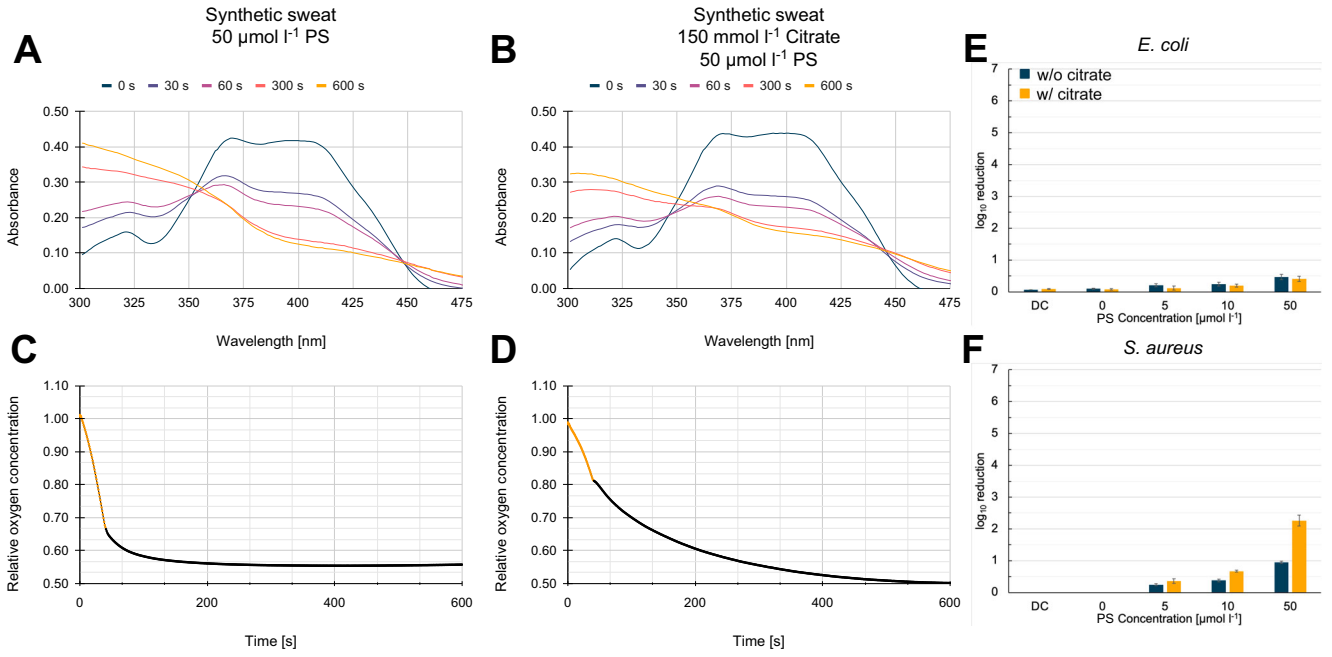

Figure 6. Investigation of the effect of synthetic sweat on the PDI. The absorption spectrum of 50 µmol L^{-1} SAPYR with synthetic sweat (A) or synthetic sweat combined with 150 mmol L^{-1} citrate (B) after different intervals of illumination with a blue light source with a radiant exposure of 18 mW cm^{-2}. Change of the oxygen concentration after 60 s of illumination with a blue light source with a radiant exposure of 18 mW cm^{-2} (indicated by yellow data points) of 50 µmol L^{-1} SAPYR with synthetic sweat (C) and synthetic sweat combined with 150 mmol L^{-1} citrate (D). PDI of *E. coli* (E) and *S. aureus* (F) in synthetic sweat with and without the addition of 150 mmol L^{-1} citrate. Error bars display the calculated standard deviation out of three independent experiments. The treatment was carried out with 18 mW cm^{-2} for 300 s, equal to 5.4 J cm^{-2}.

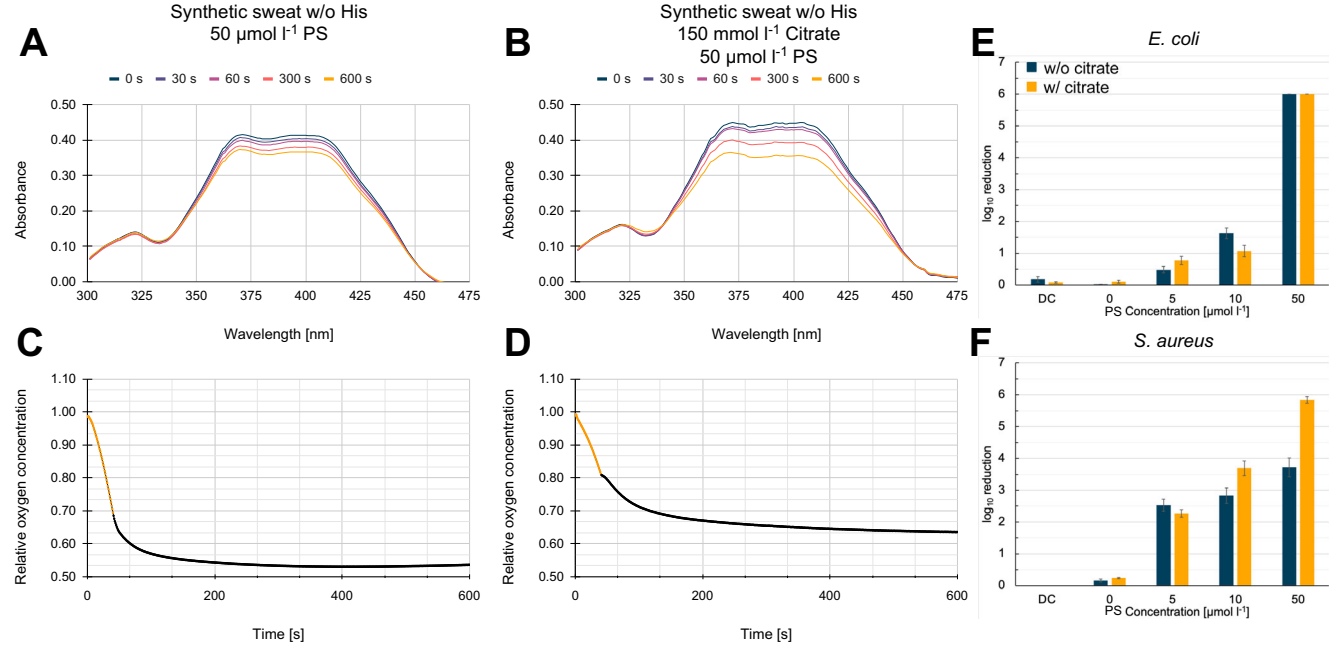

Figure 7. Investigation of the effect of synthetic sweat without histidine on the PDI. The absorption spectrum of 50 µmol L^{-1} SAPYR with synthetic sweat without histidine (A) or synthetic sweat without histidine combined with 150 mmol L^{-1} citrate (B) after different intervals of illumination with a blue light source with a radiant exposure of 18 mW cm^{-2}. Change of the oxygen concentration after 60 s of illumination with a blue light source with a radiant exposure of 18 mW cm^{-2} of 50 µmol L^{-1} SAPYR with synthetic sweat without histidine (C) or synthetic sweat without histidine combined with 150 mmol L^{-1} citrate (D). Calculated log_{10} reduction after the PDI of *E. coli* (E) and *S. aureus* (F) in synthetic sweat without histidine with and without the addition of 150 mmol L^{-1} citrate. Error bars display the calculated standard deviation out of three independent experiments. The treatment was carried out with 18 mW cm^{-2} for 300 s, equal to 5.4 J cm^{-2}.

maximum in the range of about 4 to 6 $\log_{10}$ steps in the presence of low or moderate ion concentrations. In addition, the use of citrate showed now diverse results for low and moderate ion concentrations and only a clear improvement of PDI in case of high ion concentrations (Fig. 4).

These results clearly show that the higher the concentrations of $CaCl_2$ or $MgCl_2$ in a PDI application, the more the effectiveness of PDI is impaired for both, *E. coli* and *S. aureus*. Only experiments with *E. coli* showed a clear trend for improving PDI efficacy upon adding the chelator citrate. In this case, citrate can increase efficacy especially when cells are suspended in $MgCl_2$ solutions.

The results of the present study generally confirmed that the presence of calcium or magnesium ions may hamper PDI, but differently for *E. coli* and *S. aureus*. The present findings in combination with previous studies indicate that PDI should be most effective when the concentration of such divalent ions is low or is kept low using chelating substances like citrate.

PDI and chelators

Several strategies have been already investigated by which PDI efficacy should be enhanced using different substances like the well-known EDTA. The enhancing effect of EDTA was shown, for example, *Burkholderia cepacia* by the application of a curcumin-based PS whereas EDTA was added to disorganize the cell membrane (63). The researchers could demonstrate an increased bacterial reduction in the presence of EDTA by 1 to 4 $\log_{10}$ steps depending on the treatment parameters (63), which is in good comparison to the results presented in our study. Similar results were recently obtained by another research group with *Streptococcus mutans* (64). Also, PDI with the commercially available PS photosan benefitted from the presence of EDTA (65). At present, EDTA is mainly used to facilitate the uptake of substances such as antimicrobial peptides (66–68), chlorhexidine (69,70) or quaternary ammonium compounds (71) in several bacterial species. But optimization with EDTA seems not to be favorable in all cases (72,73) and preliminary studies showed heavy PS degradation in the presence of EDTA (Figure S42).

On one hand, chelating substances can improve the uptake of substances into bacterial cells because they destabilize the bacterial membrane (74,75). On the other hand, calcium and magnesium ions are known as stabilizing factors of the outer membrane. Magnesium ions for example are also well known to bind to LPS being a major stabilizing component (76,77). Similar observations were made for calcium ions (78). Both divalent ions are known to be necessary to a certain extent to the thermodynamic stability of the outer membrane of Gram-negative bacteria (79). The outer environment of Gram-positive cells is also capable of binding magnesium or calcium ions to (wall) teichoic acids (80–82). However, a recently published study described the inhibitory effects of calcium and magnesium ions toward PDI independent of the PS used. Findings from this study did not find any differences in PS uptake in the presence of calcium or magnesium. This hints at the fact that divalent ions also a shielding effect due to electrostatic effects forcing the PS to bind to distant cell structures not vital for the survival of the bacteria (83). It might therefore be speculated that chelating agents not only destabilize the membrane but also reduce the potential shielding effect of divalent ions in PDI.

Based on the presented results, it is obvious that the effect of citrate in the presence of magnesium leads to slightly more enhanced PDI compared to calcium chloride. This is further supported by the complex formation constants which were found to be 1.88×10^{-3} for calcium citrate complexes and 2.19×10^{-3} for magnesium citrate complexes (84).

Beyond the usual destabilization mechanisms of chelating agents, PDI may benefit from another effect of these agents. PDI uses positively charged PSs to enable their electrostatic attachment to the negatively charged outside of bacterial cells. After being generated by SAPYR, the singlet oxygen molecules move by diffusion in the adjacency of the PS, hopefully reaching cellular structures of bacteria, whose oxidative damage may lead to cell death. The range of the diffusion correlates to the diffusion coefficient and the lifetime of singlet oxygen in the respective adjacency of SAPYR molecules. The lifetime in pure water is about 3.5 µs, which might be substantially shortened by any quenching mechanism, for instance when encountering cellular constituents. At the same time, the diffusion range can decrease to 100 nm or even less (85). Thus, it is of great importance that the PS molecules are getting as close as possible to bacteria by attaching to the bacterial cell at least. Any process that hampers this attachment may increase the distance between singlet oxygen and bacterial cells and therefore decrease the efficacy of PDI.

Since the LPS is one of the outermost parts of a Gram-negative bacterial cell, an electrostatic repulsion of the cationic PS should be taken into consideration. It seems that membrane stability seems to be a major factor in Gram-negatives when it comes to the binding or even the uptake of the PS. In the case of Gram-positive bacteria, it seems more likely that electrostatic repulsions, caused by the accumulation of divalent ions at teichoic acids, hinder the PS from efficiently damaging the cells *via* PDI. However, scientific literature provides different information on whether uptake or binding of cationic PS is necessary for efficient antimicrobial inactivation. While some researchers claim that cationic PSs need to be taken up by the bacterial cells (86), others state that intracellular uptake is not necessary for efficient inactivation (87). Interestingly, for the cationic PS methylene blue reports show that the presence of divalent ions inhibits the binding or uptake of the PS (86).

Further attempts in optimizing PDI of bacteria were carried out by Hamblin and co-workers demonstrating a beneficial effect of iodide, thiocyanate, azide and nitrite (88–91). The addition of antimicrobial peptides in combination with PSs has proven to be effective as well (92,93). Nonetheless, the findings concerning the inhibitory effect seem not to be ubiquitous as some PS (especially negatively charged ones) appear to have increased antimicrobial efficacy in the presence of divalent ions (94).

PDI in tap water

The results of PDI in tap water clearly showed the potential of SAPYR to inactivate Gram-negative bacteria like *E. coli* and the efficacy was even enhanced when using citrate (Fig. 5). Noteworthy, most of the bacterial contaminants in drinking water are Gram-negative representatives (95,96). In addition, the use of chelating substances allows the use of rather low SAPYR concentrations (e.g. 5 µmol L^{-1}) yielding about 3 $\log_{10}$ steps for *E. coli* although the applied tap water contained significant amounts of calcium and chloride ions. Typically, drinking water

contains calcium ions in a concentration of 0.03 to 10 mmol L^{-1} (97–100) and magnesium ions in a concentration of 0.065 to 0.62 $mmol^{-1}$ (101–103).

These inactivation efficacy differences in tap water (Fig. 5E, F), compared to the experiments carried out in calcium chloride solutions, could potentially be explained by concurring effects of various other ions in tap water (Table S1). Many of the substances in tap water remain largely uninvestigated in detail in the light of PDI, but they might bind to spaces around the bacterial envelope, consequently leading to diminished detrimental effects of the calcium ions in tap water. However, it should be noted that the tested organisms described in this study are not native to tap water but are fecal contaminants. Organisms native to drinking water such as *Legionella pneumophila*, *Mycobacterium avium* or *P. aeruginosa* are less susceptible to disinfection approaches, for example, chlorine compared to *E. coli* (104–106). These findings are in consistent with the fact that efficient PDI of microorganisms in drinking water was already demonstrated by several researchers, however, most studies had to apply higher radiant exposures. Lesar *et al*. for example demonstrated efficient PDI toward *L. pneumophila* with porphyrin-based PSs applying radiant exposures of around 12 J cm^{-2} (107,108) which is more than twice the radiant exposure compared to our study (5.4 J cm^{-2}).

PDI on skin surfaces

Tissue surfaces like skin or mucosa can be colonized by different bacteria among them also pathogens like *S. aureus* (109). In case such pathogens enter deeper skin layers due to the disruption of the skin barrier, these bacteria frequently cause skin infections. Both, colonization and infection of human skin with pathogens pose a health hazard to humans. Therefore, decolonization and the therapy of superficial skin infections is a frequent and important procedure (110), which might be a worthwhile application for PDI (36).

In case of PDI on the skin, the PS can be applied as an emulsion to the surface. Thus, the PS molecules have the chance to come into contact with the pathogens at the stratum corneum or even in deeper layers of the epidermis. Already on intact skin, the PS molecules and the generated singlet oxygen inevitably encounter not only bacteria on the skin surface but also other substances like sweat residues and terminally differentiated keratinocytes (corneocytes) of the stratum corneum. These substances may comprise different ions, residual proteins and amino acids. For instance, calcium and magnesium are particularly highly concentrated in the stratum corneum, the epidermal region with the lowest metabolism, showing concentrations of up to 30 and 70 mmol kg^{-1}, respectively (111,112). For instance, Ca^{2+} plays an important role in the regulation of keratinocyte differentiation in the epidermis and Mg^{2+} plays a role in the induction of skin barrier repair mechanisms (113,114). Also, sweat contains calcium and magnesium with concentrations ranging from 0.2 to 2 mmol L^{-1} and 0.02 to 0.4 mmol L^{-1}, respectively, but also other substances like sodium and chloride ions (115).

The results of the present study indicate that citrate can enhance PDI in the presence of synthetic sweat substances containing different ions, sodium lactate, urea and amino acids in the case of *S. aureus* (up to 2.5 log_{10} steps) but not *E. coli* (Fig. 6). Besides the fact that histidine is an effective quencher of singlet oxygen, the presence of histidine in combination with SAPYR additionally leads to a chemical alteration of the PS when illuminated. When removing histidine from the synthetic sweat solution, PDI efficacy clearly increased with increasing SAPYR concentration comparable to solutions with magnesium or calcium ions (Figs. 3 and 4) up to 6 log_{10} steps and the citrate showed again an enhancing effect. However, the inactivation data shown for experiments with synthetic sweat with or without histidine (Figs. 6E,F and 7E,F) differ from the ones obtained for tap water. A potential explanation hereby is that synthetic sweat contains less divalent ions than tap water leading to a better complexation and therefore destabilization of the cell envelope. Although the literature provides evidence that divalent ions contribute to the integrity of the cell envelope of Gram-negatives (79) as well as Gram-positives (82,116,117), these mechanisms are not fully understood yet (82).

Noteworthy, the results were achieved with rather low radiant exposure (5.4 J cm^{-2}) and low SAPYR concentration (≤50 µmol L^{-1}). Published studies already showed that PDI *in vivo* mouse models (33) or *ex vivo* human skin models (36) required higher radiant exposures and higher PS concentrations to accomplish efficient inactivation of bacteria. Due to the detrimental effect of histidine on PDI, such strategies like increased PS concentration or higher radiant exposure as well as thorough rinsing of the respective treatment site might be necessary for an application on the human skin. Nevertheless, the present results provide clear evidence that chelating substances like citrate should be added to PDI on the skin to improve the antibacterial effect.

CONCLUSION

The presented results indicate that the application of citrate can enhance the PDI influenced by certain concentrations of ionic solutions. Especially when the most abundant species are expected to be Gram-negative and concentrations of around 7.5–75 mmol L^{-1} $CaCl_2$ or $MgCl_2$ are present, the application of citrate in PDI might be beneficial. Furthermore, photodynamic treatment of tap water is efficient especially when applied against Gram-negative bacteria. In synthetic sweat, the main inhibitory substances for PDI should be amino acids like histidine followed by the ions. Nevertheless, citrate may also support the bacteria killing on skin surfaces, in particular for Gram-positive organisms like *S. aureus*, which is a major skin pathogen worldwide. The results shown in this work will serve as the basis for future research which will attempt to optimize the PDI in much more realistic environments on the human skin.

Acknowledgement—Open Access funding enabled and organized by Projekt DEAL.

SUPPORTING INFORMATION

Additional supporting information may be found online in the Supporting Information section at the end of the article:

Table S1. Composition of the tap water used for the PDI (Provided by REWAG Regensburger Energie- und Wasserversorgung AG & Co KG, Regensburg, Germany).

Table S2. Results of the statistical analysis of the microbiological inactivation data. Two conditions at a time were compared *via* unpaired, two-tailed *t*-tests assuming a normal

distribution. Events were considered statistically significant for $P < 0.001$. Not significant *P*-values are marked in red, significant *P*-values are marked in green and values exactly at the 0.001 thresholds are unmarked. The abbreviations are explained at the end of the table.

Figure S1. Emission spectrum of the used lamp and absorption spectrum of the used photosensitizer SAPYR. The *Y*-axis indicates the normalized absorption/emission while the *X*-axis indicates the wavelength in nanometre (36).

Figure S2. Absorption spectrum of 50 μmol L^{-1} SAPYR with 75 mmol L^{-1} $CaCl_2$, the dark blue line indicates the nonirradiated control, the purple line represents the dark control which was kept in the dark for 600 s and the pink line represents the sample with SAPYR irradiated for 600 s with a blue light source with a radiant exposure of 18 mW cm^{-2}.

Figure S3. Absorption spectrum of 50 μmol L^{-1} SAPYR with 75 mmol L^{-1} $MgCl_2$, the dark blue line indicates the nonirradiated control, the purple line represents the dark control which was kept in the dark for 600 s and the pink line represents the sample with SAPYR irradiated for 600 s with a blue light source with a radiant exposure of 18 mW cm^{-2}.

Figure S4. Absorption spectrum of 50 μmol L^{-1} SAPYR with 75 mmol L^{-1} $CaCl_2$ and 150 mmol L^{-1} citrate, the dark blue line indicates the nonirradiated control, the purple line represents the dark control which was kept in the dark for 600 s and the pink line represents the sample with SAPYR irradiated for 600 s with a blue light source with a radiant exposure of 18 mW cm^{-2}.

Figure S5. Absorption spectrum of 50 μmol L^{-1} SAPYR with 75 mmol L^{-1} $MgCl_2$ and 150 mmol L^{-1} citrate, the dark blue line indicates the nonirradiated control, the purple line represents the dark control which was kept in the dark for 600 s and the pink line represents the sample with SAPYR irradiated for 600 s with a blue light source with a radiant exposure of 18 mW cm^{-2}.

Figure S6. Absorption spectrum of 50 μmol L^{-1} SAPYR with tap water, the dark blue line indicates the nonirradiated control, the purple line represents the dark control which was kept in the dark for 600 s and the pink line represents the sample with SAPYR irradiated for 600 s with a blue light source with a radiant exposure of 18 mW cm^{-2}.

Figure S7. Absorption spectrum of 50 μmol L^{-1} SAPYR with tap water and 150 mmol L^{-1} citrate, the dark blue line indicates the nonirradiated control, the purple line represents the dark control which was kept in the dark for 600 s and the pink line represents the sample with SAPYR irradiated for 600 s with a blue light source with a radiant exposure of 18 mW cm^{-2}.

Figure S8. Absorption spectrum of 50 μmol L^{-1} SAPYR with synthetic sweat, the dark blue line indicates the nonirradiated control, the purple line represents the dark control which was kept in the dark for 600 s and the pink line represents the sample with SAPYR irradiated for 600 s with a blue light source with a radiant exposure of 18 mW cm^{-2}.

Figure S9. Absorption spectrum of 50 μmol L^{-1} SAPYR with synthetic sweat and 150 mmol L^{-1} citrate, the dark blue line indicates the nonirradiated control, the purple line represents the dark control which was kept in the dark for 600 s and the pink line represents the sample with SAPYR irradiated for 600 s with a blue light source with a radiant exposure of 18 mW cm^{-2}.

Figure S10. Absorption spectrum of 50 μmol L^{-1} SAPYR with synthetic sweat without histidine, the dark blue line indicates the nonirradiated control, the purple line represents the dark control which was kept in the dark for 600 s and the pink line represents the sample with SAPYR irradiated for 600 s with a blue light source with a radiant exposure of 18 mW cm^{-2}.

Figure S11. Absorption spectrum of 50 μmol L^{-1} SAPYR with synthetic sweat without histidine and 150 mmol L^{-1} citrate, the dark blue line indicates the nonirradiated control, the purple line represents the dark control which was kept in the dark for 600 s and the pink line represents the sample with SAPYR irradiated for 600 s with a blue light source with a radiant exposure of 18 mW cm^{-2}.

Figure S12. Change of the oxygen concentration in the absence of imidazole after 60 s illumination with a blue light source with a radiant exposure of 18 mW cm^{-2} in the presence of 50 μmol L^{-1} SAPYR with 75 mmol L^{-1} $CaCl_2$. The time in which the illumination was carried out is displayed as yellow datapoints. *Y*-axis indicates the relative oxygen concentration and *X*-axis the time in seconds.

Figure S13. Change of the oxygen concentration without irradiation (dark control) in the presence of 50 μmol L^{-1} SAPYR with 75 mmol L^{-1} $CaCl_2$. The time in which the illumination was carried out is displayed as yellow datapoints. *Y*-axis indicates the relative oxygen concentration and *X*-axis the time in seconds.

Figure S14. Change of the oxygen concentration after 60 s illumination with a blue light source with a radiant exposure of 18 mW cm^{-2} without PS but with 75 mmol L^{-1} $CaCl_2$ (Light control). The time in which the illumination was carried out is displayed as yellow datapoints. *Y*-axis indicates the relative oxygen concentration and *X*-axis the time in seconds.

Figure S15. Change of the oxygen concentration in the absence of imidazole after 60 s illumination with a blue light source with a radiant exposure of 18 mW cm^{-2} in the presence of 50 μmol L^{-1} SAPYR with 75 mmol L^{-1} $MgCl_2$. The time in which the illumination was carried out is displayed as yellow datapoints. *Y*-axis indicates the relative oxygen concentration and *X*-axis the time in seconds.

Figure S16. Change of the oxygen concentration without irradiation (dark control) in the presence of 50 μmol L^{-1} SAPYR with 75 mmol L^{-1} $MgCl_2$. The time in which the illumination was carried out is displayed as yellow datapoints. *Y*-axis indicates the relative oxygen concentration and *X*-axis the time in seconds.

Figure S17. Change of the oxygen concentration after 60 s illumination with a blue light source with a radiant exposure of 18 mW cm^{-2} without PS but with 75 mmol L^{-1} $MgCl_2$ (Light control). The time in which the illumination was carried out is displayed as yellow datapoints. *Y*-axis indicates the relative oxygen concentration and *X*-axis the time in seconds.

Figure S18. Change of the oxygen concentration in the absence of imidazole after 60 s illumination with a blue light source with a radiant exposure of 18 mW cm^{-2} in the presence of 50 μmol L^{-1} SAPYR with 75 mmol L^{-1} $CaCl_2$ and 150 mmol L^{-1} citrate. The time in which the illumination was carried out is displayed as yellow datapoints. *Y*-axis indicates the relative oxygen concentration and *X*-axis the time in seconds.

Figure S19. Change of the oxygen concentration without irradiation (dark control) in the presence of 50 μmol L^{-1} SAPYR with 75 mmol L^{-1} $CaCl_2$ and 150 mmol L^{-1} citrate. The time in which the illumination was carried out is displayed as yellow datapoints. *Y*-axis indicates the relative oxygen concentration and *X*-axis the time in seconds.

Figure S20. Change of the oxygen concentration after 60 s illumination with a blue light source with a radiant exposure of

18 mW cm^{-2} without PS but with 75 mmol L^{-1} $CaCl_2$ and 150 mmol L^{-1} citrate (Light control). The time in which the illumination was carried out is displayed as yellow datapoints. *Y*-axis indicates the relative oxygen concentration and *X*-axis the time in seconds.

Figure S21. Change of the oxygen concentration in the absence of imidazole after 60 s illumination with a blue light source with a radiant exposure of 18 mW cm^{-2} in the presence of 50 μmol L^{-1} SAPYR with 75 mmol L^{-1} $MgCl_2$ and 150 mmol L^{-1} citrate. The time in which the illumination was carried out is displayed as yellow datapoints. *Y*-axis indicates the relative oxygen concentration and *X*-axis the time in seconds.

Figure S22. Change of the oxygen concentration without irradiation (dark control) in the presence of 50 μmol L^{-1} SAPYR with 75 mmol L^{-1} $MgCl_2$ and 150 mmol L^{-1} citrate. The time in which the illumination was carried out is displayed as yellow datapoints. *Y*-axis indicates the relative oxygen concentration and *X*-axis the time in seconds.

Figure S23. Change of the oxygen concentration after 60 s illumination with a blue light source with a radiant exposure of 18 mW cm^{-2} without PS but with 75 mmol L^{-1} $MgCl_2$ and 150 mmol L^{-1} citrate (Light control). The time in which the illumination was carried out is displayed as yellow datapoints. *Y*-axis indicates the relative oxygen concentration and *X*-axis the time in seconds.

Figure S24. Change of the oxygen concentration in the absence of imidazole after 60 s illumination with a blue light source with a radiant exposure of 18 mW cm^{-2} in the presence of 50 μmol L^{-1} SAPYR with tap water. The time in which the illumination was carried out is displayed as yellow datapoints. *Y*-axis indicates the relative oxygen concentration and *X*-axis the time in seconds.

Figure S25. Change of the oxygen concentration without irradiation (dark control) in the presence of 50 μmol L^{-1} SAPYR with tap water. The time in which the illumination was carried out is displayed as yellow datapoints. *Y*-axis indicates the relative oxygen concentration and *X*-axis the time in seconds.

Figure S26. Change of the oxygen concentration after 60 s illumination with a blue light source with a radiant exposure of 18 mW cm^{-2} without PS but with tap water (Light control). The time in which the illumination was carried out is displayed as yellow datapoints. *Y*-axis indicates the relative oxygen concentration and *X*-axis the time in seconds.

Figure S27. Change of the oxygen concentration in the absence of imidazole after 60 s illumination with a blue light source with a radiant exposure of 18 mW cm^{-2} in the presence of 50 μmol L^{-1} SAPYR with tap water and 150 mmol L^{-1} citrate. The time in which the illumination was carried out is displayed as yellow datapoints. *Y*-axis indicates the relative oxygen concentration and *X*-axis the time in seconds.

Figure S28. Change of the oxygen concentration without irradiation (dark control) in the presence of 50 μmol L^{-1} SAPYR with tap water and 150 mmol L^{-1} citrate. The time in which the illumination was carried out is displayed as yellow datapoints. *Y*-axis indicates the relative oxygen concentration and *X*-axis the time in seconds.

Figure S29. Change of the oxygen concentration after 60 s illumination with a blue light source with a radiant exposure of 18 mW cm^{-2} without PS but with tap water and 150 mmol L^{-1} citrate (Light control). The time in which the illumination was carried out is displayed as yellow datapoints. *Y*-axis indicates the relative oxygen concentration and *X*-axis the time in seconds.

Figure S30. Change of the oxygen concentration in the absence of imidazole after 60 s illumination with a blue light source with a radiant exposure of 18 mW cm^{-2} in the presence of 50 μmol L^{-1} SAPYR and synthetic sweat. The time in which the illumination was carried out is displayed as yellow datapoints. *Y*-axis indicates the relative oxygen concentration and *X*-axis the time in seconds.

Figure S31. Change of the oxygen concentration without irradiation (dark control) in the presence of 50 μmol L^{-1} SAPYR with synthetic sweat. The time in which the illumination was carried out is displayed as yellow datapoints. *Y*-axis indicates the relative oxygen concentration and *X*-axis the time in seconds.

Figure S32. Change of the oxygen concentration after 60 s illumination with a blue light source with a radiant exposure of 18 mW cm^{-2} with synthetic sweat but without PS (Light control). The time in which the illumination was carried out is displayed as yellow datapoints. *Y*-axis indicates the relative oxygen concentration and *X*-axis the time in seconds.

Figure S33. Change of the oxygen concentration in the absence of imidazole after 60 s illumination with a blue light source with a radiant exposure of 18 mW cm^{-2} in the presence of 50 μmol L^{-1} SAPYR, synthetic sweat and 150 mmol L^{-1} citrate. The time in which the illumination was carried out is displayed as yellow datapoints. *Y*-axis indicates the relative oxygen concentration and *X*-axis the time in seconds.

Figure S34. Change of the oxygen concentration without irradiation (dark control) in the presence of 50 μmol L^{-1} SAPYR with synthetic sweat and 150 mmol L^{-1} citrate. The time in which the illumination was carried out is displayed as yellow datapoints. *Y*-axis indicates the relative oxygen concentration and *X*-axis the time in seconds.

Figure S35. Change of the oxygen concentration after 60 s illumination with a blue light source with a radiant exposure of 18 mW cm^{-2} with synthetic sweat and 150 mmol L^{-1} citrate but without PS (Light control). The time in which the illumination was carried out is displayed as yellow datapoints. *Y*-axis indicates the relative oxygen concentration and *X*-axis the time in seconds.

Figure S36. Change of the oxygen concentration in the absence of imidazole after 60 s illumination with a blue light source with a radiant exposure of 18 mW cm^{-2} in the presence of 50 μmol L^{-1} SAPYR, synthetic sweat without histidine. The time in which the illumination was carried out is displayed as yellow datapoints. *Y*-axis indicates the relative oxygen concentration and *X*-axis the time in seconds.

Figure S37. Change of the oxygen concentration without irradiation (dark control) in the presence of 50 μmol L^{-1} SAPYR with synthetic sweat without histidine. The time in which the illumination was carried out is displayed as yellow datapoints. *Y*-axis indicates the relative oxygen concentration and *X*-axis the time in seconds.

Figure S38. Change of the oxygen concentration after 60 s illumination with a blue light source with a radiant exposure of 18 mW cm^{-2} with synthetic sweat without histidine and without PS (Light control). The time in which the illumination was carried out is displayed as yellow datapoints. *Y*-axis indicates the relative oxygen concentration and *X*-axis the time in seconds.

Figure S39. Change of the oxygen concentration in the absence of imidazole after 60 s illumination with a blue light

source with a radiant exposure of 18 mW cm^{-2} in the presence of 50 µmol L^{-1} SAPYR, synthetic sweat without histidine but with 150 mmol L^{-1} citrate. The time in which the illumination was carried out is displayed as yellow datapoints. *Y*-axis indicates the relative oxygen concentration and *X*-axis the time in seconds.

Figure S40. Change of the oxygen concentration without irradiation (dark control) in the presence of 50 µmol L^{-1} SAPYR with synthetic sweat without histidine but with 150 mmol L^{-1} citrate. The time in which the illumination was carried out is displayed as yellow datapoints. *Y*-axis indicates the relative oxygen concentration and *X*-axis the time in seconds.

Figure S41. Change of the oxygen concentration after 60 s illumination with a blue light source with a radiant exposure of 18 mW cm^{-2} with synthetic sweat without histidine but with 150 mmol L^{-1} citrate and without PS (Light control). The time in which the illumination was carried out is displayed as yellow datapoints. *Y*-axis indicates the relative oxygen concentration and *X*-axis the time in seconds.

Figure S42. Absorption spectrum of SAPYR in the presence of 300 mmol L^{-1} EDTA after different intervals of illumination.

REFERENCES

1. Garner, J. S., W. R. Jarvis, T. G. Emori, T. C. Horan and J. M. Hughes (1988) CDC definitions for nosocomial infections, 1988. *AJIC Am. J. Infect. Control* **16**, 128–140.
2. Cassini, A., L. D. Högberg, D. Plachouras, A. Quattrocchi, A. Hoxha, G. S. Simonsen, M. Colomb-Cotinat, M. E. Kretzschmar, B. Devleesschauwer, M. Cecchini, D. A. Ouakrim, T. C. Oliveira, M. J. Struelens, C. Suetens, D. L. Monnet, R. Strauss, K. Mertens, T. Struyf, B. Catry, K. Latour, I. N. Ivanov, E. G. Dobreva, A. Tambic Andraševic, S. Soprek, A. Budimir, N. Paphitou, H. Žemlicková, S. Schytte Olsen, U. Wolff Sönksen, P. Märtin, M. Ivanova, O. Lyytikäinen, J. Jalava, B. Coignard, T. Eckmanns, M. Abu Sin, S. Haller, G. L. Daikos, A. Gikas, S. Tsiodras, F. Kontopidou, Á. Tóth, Á. Hajdu, Ó. Guólaugsson, K. G. Kristinsson, S. Murchan, K. Burns, P. Pezzotti, C. Gagliotti, U. Dumpis, A. Liuimiene, M. Perrin, M. A. Borg, S. C. de Greeff, J. C. Monen, M. B. Koek, P. Elstrøm, D. Zabicka, A. Deptula, W. Hryniewicz, M. Caniça, P. J. Nogueira, P. A. Fernandes, V. Manageiro, G. A. Popescu, R. I. Serban, E. Schréterová, S. Litvová, M. Štefkovicová, J. Kolman, I. Klavs, A. Korošec, B. Aracil, A. Asensio, M. Pérez-Vázquez, H. Billström, S. Larsson, J. S. Reilly, A. Johnson and S. Hopkins (2019) Attributable deaths and disability-adjusted life-years caused by infections with antibiotic-resistant bacteria in the EU and the European Economic Area in 2015: A population-level modelling analysis. *Lancet Infect. Dis.* **19**, 56–66.
3. European Centre for Disease Prevention and Control (2008) European Centre for Disease Prevention and Control: Annual epidemiological report on communicable diseases in Europe 2008.
4. Claus, F., A. Sachse and W. Ried (2014) Volkswirtschaftliche Kosten von MRSA in Deutschland. *Gesundheitswesen* **76**, 800–806.
5. Allegranzi, B., S. B. Nejad, C. Combescure, W. Graafmans, H. Attar, L. Donaldson and D. Pittet (2011) Burden of endemic health-care-associated infection in developing countries: Systematic review and meta-analysis. *Lancet* **377**, 228–241.
6. Mehta, Y., A. Gupta, S. Todi, S. N. Myatra, D. P. Samaddar, V. Patil, P. K. Bhattacharya and S. Ramasubban (2014) Guidelines for prevention of hospital acquired infections. *Indian J. Crit. Care Med.* **18**, 149–163.
7. Clancy, C., T. Delungahawatta and C. P. Dunne (2021) Hand hygiene-related clinical trials reported between 2014 and 2020: A comprehensive systematic review. *J. Hosp. Infect* **111**, 6–26.
8. Carling, P. C., M. M. Parry, M. E. Rupp, J. L. Po, B. Dick, S. Von Beheren and Group, H. E. H. S (2008) Improving cleaning of the environment surrounding patients in 36 acute care hospitals. *Infect. Control Hosp. Epidemiol.* **29**, 1035–1041.
9. Klein, E. Y., M. Milkowska-Shibata, K. K. Tseng, M. Sharland, S. Gandra, C. Pulcini and R. Laxminarayan (2021) Assessment of WHO antibiotic consumption and access targets in 76 countries, 2000–15: An analysis of pharmaceutical sales data. *Lancet Infect. Dis.* **21**, 107–115.
10. Wainwright, M., T. Maisch, S. Nonell, K. Plaetzer, A. Almeida, G. P. Tegos and M. R. Hamblin (2017) Photoantimicrobials—Are we afraid of the light? *Lancet Infect. Dis.* **17**, e49–e55.
11. Tavares, A., C. M. B. Carvalho, M. A. Faustino, M. G. P. M. S. Neves, J. P. C. Tomé, A. C. Tomé, J. A. S. Cavaleiro, Â. Cunha, N. C. M. Gomes, E. Alves and A. Almeida (2010) Antimicrobial photodynamic therapy: Study of bacterial recovery viability and potential development of resistance after treatment. *Mar. Drugs* **8**, 91–105.
12. Marasini, S., L. G. Leanse and T. Dai (2021) Can microorganisms develop resistance against light based anti-infective agents? *Adv. Drug Deliv. Rev.* **175**, 113822.
13. Hamblin, M. R. (2016) Antimicrobial photodynamic inactivation: A bright new technique to kill resistant microbes. *Curr. Opin. Microbiol.* **33**, 67–73.
14. Eckl, D. B., L. Dengler, M. Nemmert, A. Eichner, W. Bäumler and H. Huber (2018) A closer look at dark toxicity of the photosensitizer TMPyP in bacteria. *Photochem. Photobiol.* **94**, 165–172.
15. Majiya, H., K. F. Chowdhury, N. J. Stonehouse and P. Millner (2019) TMPyP functionalised chitosan membrane for efficient sunlight driven water disinfection. *J. Water Process Eng.* **30**, 100475.
16. Ergaieg, K. and R. Seux (2009) A comparative study of the photoinactivation of bacteria by meso-substituted cationic porphyrin, rose Bengal and methylene blue. *Desalination* **246**, 353–362.
17. Almeida, J., J. P. C. Tomé, M. G. P. M. S. Neves, A. C. Tomé, J. A. S. Cavaleiro, Â. Cunha, L. Costa, M. A. F. Faustino and A. Almeida (2014) Photodynamic inactivation of multidrug-resistant bacteria in hospital wastewaters: Influence of residual antibiotics. *Photochem. Photobiol. Sci.* **13**, 626–633.
18. Eichner, A., T. Holzmann, D. B. Eckl, F. Zeman, M. Koller, M. Huber, S. Pemmerl, W. Schneider-Brachert and W. Bäumler (2020) Novel photodynamic coating reduces the bioburden on near-patient surfaces thereby reducing the risk for onward pathogen transmission: A field study in two hospitals. *J. Hosp. Infect.* **104**, 85–91.
19. Humphreys, H. (2014) Self-disinfecting and microbiocide-impregnated surfaces and fabrics: What potential in interrupting the spread of healthcare-associated infection? *Clin. Infect. Dis.* **58**, 848–853.
20. Bäumler, W., D. Eckl, T. Holzmann and W. Schneider-Brachert (2021) Antimicrobial coatings for environmental surfaces in hospitals: A potential new pillar for prevention strategies in hygiene. *Crit. Rev. Microbiol.* **48**, 531–564.
21. Kalb, L., P. Bäßler, W. Schneider-Brachert and D. B. Eckl (2022) Antimicrobial photodynamic coatings reduce the microbial burden on environmental surfaces in public transportation – A field study in buses. *Int. J. Environ. Res. Public Health* **19**, 2325.
22. Baigorria, E., J. E. Durantini, S. R. Martínez, M. E. Milanesio, Y. B. Palacios and A. M. Durantini (2021) Potentiation effect of iodine species on the antimicrobial capability of surfaces coated with electroactive phthalocyanines. *ACS Appl. Bio Mater.* **4**, 8559–8570.
23. Rosenberg, M., K. Ilić, K. Juganson, A. Ivask, M. Ahonen, I. V. Vrček and A. Kahru (2019) Potential ecotoxicological effects of antimicrobial surface coatings: A literature survey backed up by analysis of market reports. *PeerJ* **7**, e6315.
24. Adlhart, C., J. Verran, N. F. Azevedo, H. Olmez, M. M. Keinänen-Toivola, I. Gouveia, L. F. Melo and F. Crijns (2018) Surface modifications for antimicrobial effects in the healthcare setting: A critical overview. *J. Hosp. Infect.* **99**, 239–249.
25. Cieplik, F., A. Späth, J. Regensburger, A. Gollmer, L. Tabenski, K. A. Hiller, W. Bäumler, T. Maisch and G. Schmalz (2013) Photodynamic biofilm inactivation by SAPYR – An exclusive singlet oxygen photosensitizer. *Free Radic. Biol. Med.* **65**, 477–487.
26. Späth, A., C. Leibl, F. Cieplik, K. Lehner, J. Regensburger, K. A. Hiller, W. Bäumler, G. Schmalz and T. Maisch (2014) Improving photodynamic inactivation of bacteria in dentistry: Highly effective and fast killing of oral key pathogens with novel tooth-colored type-II photosensitizers. *J. Med. Chem.* **57**, 5157–5168.

27. Eichner, A., A. Gollmer, A. Späth, W. Bäumler, J. Regensburger, B. König and T. Maisch (2015) Fast and effective inactivation of *Bacillus atrophaeus* endospores using light-activated derivatives of vitamin B2. *Photochem. Photobiol. Sci.* **14**, 387–396.
28. Tabenski, I., F. Cieplik, L. Tabenski, J. Regensburger, K.-A. Hiller, W. Buchalla, T. Maisch and A. Späth (2016) The impact of cationic substituents in phenalen-1-one photosensitizers on antimicrobial photodynamic efficacy. *Photochem. Photobiol. Sci.* **15**, 57–68.
29. Muehler, D., K. Sommer, S. Wennige, K.-A. Hiller, F. Cieplik, T. Maisch and A. Späth (2017) Light-activated phenalen-1-one bactericides: Efficacy, toxicity and mechanism compared with benzalkonium chloride. *Future Microbiol.* **12**, 1297–1310.
30. Späth, A., A. Graeler, T. Maisch and K. Plaetzer (2018) CureCuma–cationic curcuminoids with improved properties and enhanced antimicrobial photodynamic activity. *Eur. J. Med. Chem.* **159**, 423–440.
31. Eckl, D. B., H. Huber and W. Bäumler (2020) First report on photodynamic inactivation of archaea including a novel method for high-throughput reduction measurement. *Photochem. Photobiol.* **96**, 883–889.
32. Cieplik, F., F. Wimmer, D. Muehler, T. Thurnheer, G. N. Belibasakis, K.-A. Hiller, T. Maisch and W. Buchalla (2018) Phenalen-1-one-mediated antimicrobial photodynamic therapy and chlorhexidine applied to a novel caries biofilm model. *Caries Res.* **52**, 447–453.
33. Ragàs, X., T. Dai, G. P. Tegos, M. Agut, S. Nonell and M. R. Hamblin (2010) Photodynamic inactivation of *Acinetobacter baumannii* using phenothiazinium dyes: *In vitro* and *in vivo* studies. *Lasers Surg. Med.* **42**, 384–390.
34. Zolfaghari, P. S., S. Packer, M. Singer, S. P. Nair, J. Bennett, C. Street and M. Wilson (2009) *In vivo* killing of *Staphylococcus aureus* using a light-activated antimicrobial agent. *BMC Microbiol.* **9**, 1–8.
35. Hamblin, M. R., D. A. O'Donnell, N. Murthy, C. H. Contag and T. Hasan (2002) Rapid control of wound infections by targeted photodynamic therapy monitored by *in vivo* bioluminescence imaging. *Photochem. Photobiol.* **75**, 51–57.
36. Schreiner, M., W. Bäumler, D. B. Eckl, A. Späth, B. König and A. Eichner (2018) Photodynamic inactivation of bacteria to decolonize meticillin-resistant *Staphylococcus aureus* from human skin. *Br. J. Dermatol.* **179**, 1358–1367.
37. Sato, K., W. H. Kang, K. Saga and K. T. Sato (1989) Biology of sweat glands and their disorders. I. Normal sweat gland function. *J. Am. Acad. Dermatol.* **20**, 537–563.
38. Patterson, M. J., S. D. R. Galloway and M. A. Nimmo (2000) Variations in regional sweat composition in normal human males. *Exp. Physiol.* **85**, 869–875.
39. Eckl, D. B., S. S. Eben, L. Schottenhaml, A. Eichner, R. Vasold, A. Späth, W. Bäumler and H. Huber (2021) Interplay of phosphate and carbonate ions with flavin photosensitizers in photodynamic inactivation of bacteria. *PLoS One* **16**, e0253212.
40. Gerba, C. P., C. Wallis and J. L. Melnick (1977) Disinfection of wastewater by photodynamic oxidation. *J. Water Pollut. Control Fed.* **49**, 575–583.
41. Bartolomeu, M., S. Reis, M. Fontes, M. G. P. M. S. Neves, M. A. F. Faustino and A. Almeida (2017) Photodynamic action against wastewater microorganisms and chemical pollutants: An effective approach with low environmental impact. *Water* **9**, 630.
42. Bartolomeu, M., C. Oliveira, C. Pereira, M. G. P. M. S. Neves, M. A. F. Faustino and A. Almeida (2021) Antimicrobial photodynamic approach in the inactivation of viruses in wastewater: Influence of alternative adjuvants. *Antibiotics* **10**, 767.
43. Rossi, G., D. Goi and C. Comuzzi (2012) The photodynamic inactivation of *Staphylococcus aureus* in water using visible light with a new expanded porphyrin. *J. Water Health* **10**, 390–399.
44. Kuznetsova, N. A., D. A. Makarov, O. L. Kaliya and G. N. Vorozhtsov (2007) Photosensitized oxidation by dioxygen as the base for drinking water disinfection. *J. Hazard. Mater.* **146**, 487–491.
45. Obara, H., M. Takeuchi, H. Kawakubo, M. Shinoda, K. Okabayashi, K. Hayashi, Y. Sekimoto, Y. Maeda, T. Kondo, Y. Sato and Y. Kitagawa (2020) Aqueous olanexidine versus aqueous povidone-iodine for surgical skin antisepsis on the incidence of surgical site infections after clean-contaminated surgery: A multicentre, prospective, blinded-endpoint, randomised controlled trial. *Lancet Infect. Dis.* **20**, 1281–1289.
46. Krishna, B. V. S. and A. P. Gibb (2010) Use of octenidine dihydrochloride in meticillin-resistant *Staphylococcus aureus* decolonisation regimens: A literature review. *J. Hosp. Infect.* **74**, 199–203.
47. Williamson, D. A., G. P. Carter and B. P. Howden (2017) Current and emerging topical antibacterials and antiseptics: Agents, action, and resistance patterns. *Clin. Microbiol. Rev.* **30**, 827–860.
48. Boretti, A. and L. Rosa (2019) Reassessing the projections of the world water development report. *NPJ Clean Water* **2**, 1–6.
49. Li, X.-F. and W. A. Mitch (2018) Drinking water disinfection byproducts (DBPs) and human health effects: Multidisciplinary challenges and opportunities. *Environ. Sci. Technol.* **52**, 1681–1689.
50. Lambrechts, S. A. G., M. C. G. Aalders, D. H. Langeveld-Klerks, Y. Khayali and J. W. M. Lagerberg (2004) Effect of monovalent and divalent cations on the photoinactivation of bacteria with meso-substituted cationic porphyrins. *Photochem. Photobiol.* **79**, 297–302.
51. Kato, N., M. Ohta, N. Kido, H. Ito and S. Naito (1988) Formation of a hexagonal lattice structure by an R-form lipopolysaccharide of *Klebsiella* sp. *Microbiol. Immunol.* **32**, 481–490.
52. Rojas, E. R., G. Billings, P. D. Odermatt, G. K. Auer, L. Zhu, A. Miguel, F. Chang, D. B. Weibel, J. A. Theriot and K. C. Huang (2018) The outer membrane is an essential load-bearing element in gram-negative bacteria. *Nature* **559**, 617–621.
53. Mueller, J. H. and J. Hinton (1941) A protein-free medium for primary isolation of the *Gonoeceus* and *meningococcus*. *Proc. Soc. Exp. Biol. Med.* **48**, 330–333.
54. Schaal, S., K. Kunsch and S. Kunsch (2016) Der Mensch in Zahlen. https://doi.org/10.1007/978-3-642-55399-8
55. Callewaert, C., B. Buysschaert, E. Vossen, V. Fievez, T. Van de Wiele and N. Boon (2014) Artificial sweat composition to grow and sustain a mixed human axillary microbiome. *J. Microbiol. Methods* **103**, 6–8.
56. REWAG. Unser Trinkwasser und seine Bestandteile.
57. Hartman, P. E., Z. Hartman and K. T. Ault (1990) Scavening of singlet molecular oxygen by imidazole compounds: High and sustained activities of carboxy terminal histidine dipeptides and exceptional activity of imidazole-4-acetic acid. *Photochem. Photobiol.* **51**, 59–66.
58. Maisch, T., J. Baier, B. Franz, M. Maier, M. Landthaler, R.-M. Szeimies and W. Bäumler (2007) The role of singlet oxygen and oxygen concentration in photodynamic inactivation of bacteria. *Proc. Natl. Acad. Sci. U.S.A.* **104**, 7223–7228.
59. Bechert, T., P. Steinrücke and J. P. Guggenbichler (2000) A new method for screening anti-infective biomaterials. *Nat. Med.* **6**, 1053–1056.
60. Fabritius, M., A. A. Al-Munajjed, C. Freytag, H. Jülke, M. Zehe, T. Lemarchand, J. J. Arts, D. Schumann, V. Alt and K. Sternberg (2020) Antimicrobial silver multilayer coating for prevention of bacterial colonization of orthopedic implants. *Materials (Basel)* **13**, 1415.
61. Boyce, J. M. and D. Pittet (2002) Guideline for hand hygiene in health-care settings. Recommendations of the Healthcare Infection Control Practices Advisory Committee and the HICPAC/SHEA/APIC/IDSA Hand Hygiene Task Force. *Infect. Control Hosp. Epidemiol.* **23**, 3–40.
62. Thomas, O. and V. Cerda (2007) From spectra to qualitative and quantitative results. In *UV-Visible Spectrophotometry of Water and Wastewater* (Edited by O. Thomas and C. Burgess), pp. 31–33. Elsevier B.V, Amsterdam.
63. Hu, J., S. Lin, B. K. Tan, S. S. Hamzah, Y. Lin, Z. Kong, Y. Zhang, B. Zheng and S. Zeng (2018) Photodynamic inactivation of *Burkholderia cepacia* by curcumin in combination with EDTA. *Food Res. Int.* **111**, 265–271.
64. Nima, G., J. Soto-Montero, L. A. Alves, R. O. Mattos-Graner and M. Giannini (2021) Photodynamic inactivation of *Streptococcus mutans* by curcumin in combination with EDTA. *Dent. Mater.* **37**, e1–e14.
65. Maisch, T., J. Wagner, V. Papastamou, H. J. Nerl, K. A. Hiller, R. M. Szeimies and G. Schmalz (2009) Combination of 10% EDTA, Photosan, and a blue light hand-held photopolymerizer to inactivate leading oral bacteria in dentistry *in vitro*. *J. Appl. Microbiol.* **107**, 1569–1578.

66. Khan, A., K. D. Vu, B. Riedl and M. Lacroix (2015) Optimization of the antimicrobial activity of nisin, Na-EDTA and pH against gram-negative and gram-positive bacteria. *LWT – Food Sci. Technol.* **61**, 124–129.
67. Mastromatteo, M., A. Lucera, M. Sinigaglia and M. R. Corbo (2010) Synergic antimicrobial activity of lysozyme, nisin, and EDTA against *Listeria monocytogenes* in ostrich meat patties. *J. Food Sci.* **75**, M422–M429.
68. Sawer, I. K., M. I. Berry and J. L. Ford (1997) Effect of medium composition, agitation and the presence of EDTA on the antimicrobial activity of cryptolepine. *Lett. Appl. Microbiol.* **25**, 207–211.
69. Guardabassi, L., G. Ghibaudo and P. Damborg (2010) *In vitro* antimicrobial activity of a commercial ear antiseptic containing chlorhexidine and Tris–EDTA. *Vet. Dermatol.* **21**, 282–286.
70. Jalil, A., M. H. Asim, Z. B. Akkus, M. Schoenthaler, B. Matuszczak and A. Bernkop-Schnürch (2019) Self-emulsifying drug delivery systems comprising chlorhexidine and alkyl-EDTA: A novel approach for augmented antimicrobial activity. *J. Mol. Liq.* **295**, 111649.
71. Lambert, R. J. W., G. W. Hanlon and S. P. Denyer (2004) The synergistic effect of EDTA/antimicrobial combinations on *Pseudomonas aeruginosa*. *J. Appl. Microbiol.* **96**, 244–253.
72. Bertoloni, G., B. Salvato, M. Dall'Acqua, M. Vazzoler and G. Jori (1984) Hematoporphyrin-sensitized photoinactivation of *Streptococcus faecalis*. *Photochem. Photobiol.* **39**, 811–816.
73. Bertolini, G., F. Rossi, G. Valduga, G. Jori and J. Van Lier (1990) Photosensitizing activity of water- and lipid-soluble phthalocyanines on *Escherichia coli*. *FEMS Microbiol. Lett.* **71**, 149–155.
74. Birdsell, D. C. and E. H. Cota-Robles (1967) Production and ultrastructure of lysozyme and ethylenediaminetetraacetate-lysozyme spheroplasts of *Escherichia coli*. *J. Bacteriol.* **93**, 427–437.
75. Costerton, W., J. Cecil, I. Forsberg, A. Matula Tibor, F. L. Buckmire and A. MacLeod Robert (1967) Nutrition and metabolism of marine bacteria XVI. Formation of protoplasts, Spheroplasts, and related forms from a gram-negative marine bacterium. *J. Bacteriol.* **94**, 1764–1777.
76. Hughes, M. N. and R. K. Poole (1991) Metal speciation and microbial growth—The hard (and soft) facts. *Microbiology* **137**, 725–734.
77. Walker, G. M. (1994) The roles of magnesium in biotechnology. *Crit. Rev. Biotechnol.* **14**, 311–354.
78. Clifton, L. A., M. W. A. Skoda, A. P. Le Brun, F. Ciesielski, I. Kuzmenko, S. A. Holt and J. H. Lakey (2015) Effect of divalent cation removal on the structure of gram-negative bacterial outer membrane models. *Langmuir* **31**, 404–412.
79. Hancock, R. E. W. (1984) Alterations in outer membrane permeability. *Annu. Rev. Microbiol.* **38**, 237–264.
80. Lambert, P. A., I. C. Hancock and J. Baddiley (1975) Influence of alanyl ester residues on the binding of magnesium ions to teichoic acids. *Biochem. J.* **151**, 671–676.
81. Thomas, K. J. and C. V. Rice (2015) Equilibrium binding behavior of magnesium to wall teichoic acid. *Biochim. Biophys. Acta Biomembr.* **1848**, 1981–1987.
82. Thomas, K. J., 3rd and C. V. Rice (2014) Revised model of calcium and magnesium binding to the bacterial cell wall. *Biometals* **27**, 1361–1370.
83. Eckl, D. B., N. Landgraf, A. K. Hoffmann, L. Schottenhaml, J. Dirscherl, N. Weber, S. S. Eben, P. Bäßler, A. Eichner, H. Huber and W. Bäumler (2022) Inhibitory effects of calcium or magnesium ions on PDI. *J. Photochem. Photobiol.* **11**, 100122.
84. Meyer, J. L. (1974) Formation constants for interaction of citrate with calcium and magnesium lons. *Anal. Biochem.* **62**, 295–300.
85. Hatz, S., L. Poulsen and P. R. Ogilby (2008) Time-resolved singlet oxygen phosphorescence measurements from photosensitized experiments in single cells: Effects of oxygen diffusion and oxygen concentration. *Photochem. Photobiol.* **84**, 1284–1290.
86. George, S., M. R. Hamblin and A. Kishen (2009) Uptake pathways of anionic and cationic photosensitizers into bacteria. *Photochem. Photobiol. Sci.* **8**, 788–795.
87. Preuß, A., L. Zeugner, S. Hackbarth, M. A. F. Faustino, M. G. P. M. S. Neves, J. A. S. Cavaleiro and B. Roeder (2013) Photoinactivation of *Escherichia coli* (SURE2) without intracellular uptake of the photosensitizer. *J. Appl. Microbiol.* **114**, 36–43.
88. Yuan, L., P. Lyu, Y. Y. Huang, N. Du, W. Qi, M. R. Hamblin and Y. Wang (2020) Potassium iodide enhances the photobactericidal effect of methylene blue on *Enterococcus faecalis* as planktonic cells and as biofilm infection in teeth. *J. Photochem. Photobiol. B Biol.* **203**, 111730.
89. Huang, L., G. Szewczyk, T. Sarna and M. R. Hamblin (2017) Potassium iodide potentiates broad-Spectrum antimicrobial photodynamic inactivation using Photofrin. *ACS Infect. Dis.* **3**, 320–328.
90. Hamblin, M. R. (2017) Potentiation of antimicrobial photodynamic inactivation by inorganic salts. *Expert Rev. Anti Infect. Ther.* **15**, 1059–1069.
91. Huang, L., T. G. St. Denis, Y. Xuan, Y. Y. Huang, M. Tanaka, A. Zadlo, T. Sarna and M. R. Hamblin (2012) Paradoxical potentiation of methylene blue-mediated antimicrobial photodynamic inactivation by sodium azide: Role of ambient oxygen and azide radicals. *Free Radic. Biol. Med.* **53**, 2062–2071.
92. de Freitas, L. M., E. N. Lorenzón, N. A. Santos-Filho, L. H. de Zago, M. P. Uliana, K. T. de Oliveira, E. M. Cilli and C. R. Fontana (2018) Antimicrobial photodynamic therapy enhanced by the peptide aurein 1.2. *Sci. Rep.* **8**, 4212.
93. Zhou, J., G.-B. Qi and H. Wang (2016) A purpurin-peptide derivative for selective killing of gram-positive bacteria via insertion into cell membrane. *J. Mater. Chem. B* **4**, 4855–4861.
94. Gsponer, N. S., M. B. Spesia and E. N. Durantini (2015) Effects of divalent cations, EDTA and chitosan on the uptake and photoinactivation of *Escherichia coli* mediated by cationic and anionic porphyrins. *Photodiagnosis Photodyn. Ther.* **12**, 67–75.
95. Cabral, J. P. S. (2010) Water microbiology. Bacterial pathogens and water. *Int. J. Environ. Res. Public Health* **7**, 3657–3703.
96. Ford, T. E. (1999) Microbiological safety of drinking water: United States and global perspectives. *Environ. Health Perspect.* **107**, 191–206.
97. Azoulay, A., P. Garzon and M. J. Eisenberg (2001) Comparison of the mineral content of tap water and bottled waters. *J. Gen. Intern. Med.* **16**, 168–175.
98. Cotruvo, J. and J. Bartram (2009) *Calcium and Magnesium in Drinking-Water: Public Health Significance*. World Health Organization, Geneva.
99. Kumar, M., S. Singh and R. K. Mahajan (2006) Trace level determination of U, Zn, Cd, Pb and Cu in drinking water samples. *Environ. Monit. Assess.* **112**, 283–292.
100. Al-Saleh, I. and I. Al-Doush (1998) Survey of trace elements in household and bottled drinking water samples collected in Riyadh, Saudi Arabia. *Sci. Total Environ.* **216**, 181–192.
101. Rylander, R., H. Bonevik and E. Rubenowitz (1991) Magnesium and calcium in drinking water and cardiovascular mortality. *Scand. J. Work Environ. Health* **17**, 91–94.
102. Rubenowitz, E., G. Axelsson and R. Rylander (1998) Magnesium in drinking water and body magnesium status measured using an oral loading test. *Scand. J. Clin. Lab. Invest.* **58**, 423–428.
103. Rubenowitz, E., G. Axelsson and R. Rylander (1996) Magnesium in drinking water and death from acute myocardial infarction. *Am. J. Epidemiol.* **143**, 456–462.
104. Kuchta, J. M., S. J. States, J. E. McGlaughlin, J. H. Overmeyer, R. M. Wadowsky, A. M. McNamara, R. S. Wolford and R. B. Yee (1985) Enhanced chlorine resistance of tap water-adapted Legionella pneumophila as compared with agar medium-passaged strains. *Appl. Environ. Microbiol.* **50**, 21–26.
105. Taylor, R. H., J. O. Falkinham III, C. D. Norton and M. W. LeChevallier (2000) Chlorine, chloramine, chlorine dioxide, and ozone susceptibility of Mycobacterium avium. *Appl. Environ. Microbiol.* **66**, 1702–1705.
106. Grobe, S., J. Wingender and H.-C. Flemming (2001) Capability of mucoid Pseudomonas aeruginosa to survive in chlorinated water. *Int. J. Hyg. Environ. Health* **204**, 139–142.
107. Lesar, A., M. Mušković, G. Begić, M. Lončarić, D. Tomić Linšak, N. Malatesti and I. Gobin (2020) Cationic porphyrins as effective agents in photodynamic inactivation of opportunistic plumbing pathogen *Legionella pneumophila*. *Int. J. Mol. Sci.* **21**, 5367.
108. Lesar, A., G. Begić, N. Malatesti and I. Gobin (2019) Innovative approach in *legionella* water treatment with photodynamic cationic amphiphilic porphyrin. *Water Supply* **19**, 1473–1479.
109. Lee, A. S., H. de Lencastre, J. Garau, J. Kluytmans, S. Malhotra-Kumar, A. Peschel and S. Harbarth (2018) Methicillin-resistant Staphylococcus aureus. *Nat. Rev. Dis. Prim.* **4**, 18033.

110. Kuraitis, D. and L. Williams (2018) Decolonization of *Staphylococcus aureus* in healthcare: A dermatology perspective. *J. Healthc. Eng*. **2018**, 2382050.
111. Forslind, B., M. Lindberg, G. M. Roomans, J. Pallon and Y. Werner-Linde (1997) Aspects on the physiology of human skin: Studies using particle probe analysis. *Microsc. Res. Tech.* **38**, 373–386.
112. Von Zglinicki, T., M. Lindberg, G. M. Roomans and B. Forslind (1993) Water and ion distribution profiles in human skin. *Acta Derm. Venereol.* **73**, 340–343.
113. Denda, M., J. Hosoi and Y. Asida (2000) Visual imaging of ion distribution in human epidermis. *Biochem. Biophys. Res. Commun.* **272**, 134–137.
114. Tu, C.-L. and D. D. Bikle (2013) Role of the calcium-sensing receptor in calcium regulation of epidermal differentiation and function. *Best Pract. Res. Clin. Endocrinol. Metab.* **27**, 415–427.
115. Baker, L. B. and A. S. Wolfe (2020) Physiological mechanisms determining eccrine sweat composition. *Eur. J. Appl. Physiol.* **120**, 719–752.
116. Doyle, R. J., T. H. Matthews and U. N. Streips (1980) Chemical basis for selectivity of metal ions by the *Bacillus subtilis* cell wall. *J. Bacteriol.* **143**, 471–480.
117. Yee, N., D. A. Fowle and F. G. Ferris (2004) A Donnan potential model for metal sorption onto *Bacillus subtilis*. *Geochim. Cosmochim. Acta* **68**, 3657–3664.